Thermal history of potential gas reservoir rocks in the eastern Parnaíba Basin, Brazil

Márcio Cardoso Jr., Farid Chemale Jr., Christie H. Engelmann de Oliveira, Carlos Emanoel de Souza Cruz, Carlos Jorge de Abreu, and Frederico Antonio Genezini

ABSTRACT

The Parnaíba Basin is a major intracratonic sedimentary basin in Brazil with unconventional petroleum systems as a potential natural resource formed by the influence of igneous intrusions. To constrain the thermal history of unexplored potential reservoir rocks in the eastern part of the Parnaíba Basin, sedimentary rocks near intrusions were analyzed by petrography and thermochronology (apatite fission-track [AFT] and zircon fission-track [ZFT] dating). Petrography shows grain dissolution and carbonate pore filling generated by thermal destabilization of feldspars. The AFT results indicate partial annealing by the last magmatic event in the basin, and ZFT results show ages of maximum paleotemperature compatible with the Sardinha magmatic event (120–130 Ma). In thermal history models, rocks close to intrusions experienced maximum paleotemperatures above 300°C, which is higher than what is considered favorable for reservoir rocks. Hydrothermal fluids modified the diagenetic evolution of the succession by dissolving and precipitating carbonate cement in pore spaces. In the studied area, at distances greater than 50 m (>164 ft) from the intrusion, the rocks were not substantially altered, and in terms of paleotemperature, they can be considered potentially viable reservoirs. The thermal history analysis of potential tight gas sandstone reservoirs affected by intrusive bodies is valuable for characterizing the thermal enhancement or destruction of the reservoir's qualities.

Manuscript received May 16, 2018; provisional acceptance July 31, 2018; revised manuscript received October 1, 2018; revised manuscript provisional acceptance November 13, 2018; 2nd revised manuscript received December 13, 2018; 2nd revised manuscript provisional acceptance January 15, 2019; 3rd revised manuscript received February 7, 2019; final acceptance May 2, 2019.
DOI:10.1306/05021918117

AUTHORS

Márcio Cardoso Jr. ~ *Programa de Pós-Graduação em Geologia, Universidade do Vale do Rio dos Sinos (UNISINOS), São Leopoldo, Rio Grande do Sul, Brazil; marciocard@edu.unisinos.br*

Márcio Cardoso Jr. is a researcher in the geology department at UNISINOS. He received his B.S and M.S. from UNISINOS. His research interests are in petroleum geology and sedimentary basin evolution, with a focus on thermochronology and stratigraphic modeling.

Farid Chemale Jr. ~ *Programa de Pós-Graduação em Geologia, UNISINOS, São Leopoldo, Rio Grande do Sul, Brazil; faridcj@unisinos.br, faridchemale@gmail.com*

Farid Chemale Jr. is an expert on tectonics and holds a B.S. degree from UNISINOS, an M.S. degree from Universidade Federal do Rio Grande do Sul (UFRGS), and a Ph.D. from Technical University Clausthal. He is currently professor of the geology graduate program at UNISINOS, and he has previously taught at the University of Brasília, Ouro Preto and Rio Grande do Sul. He has written 185 research papers focused on tectonics, stratigraphy, geochemistry, and isotope studies.

Christie H. Engelmann de Oliveira ~ *Programa de Pós-Graduação em Geologia, UNISINOS, São Leopoldo, Rio Grande do Sul, Brazil; christie.oliveira10@gmail.com*

Christie H. Engelmann de Oliveira is a postdoctoral researcher in geology. She received a B.S. degree and a Ph.D. from UFRGS and an M.S. degree from Universidade de Brasília. Her research interests include basin analysis, geochronology, and thermochronology, with a particular focus on the study of tectonic evolution of sedimentary basins, petroleum geology, and multidisciplinary sediment provenance analysis.

Carlos Emanoel de Souza Cruz ~ *Instituto de Geociências, Universidade de Brasília, Brasília, Federal District, Brazil; souzacruz@unb.br*

Carlos E. de Souza Cruz spent 35 years at Petrobras working on many integrated geological and geophysical projects in many areas of the world before joining the Universidade de Brasília in August 2014 as an adjunct professor. His expertise includes sedimentary basin analysis, reservoir studies, prospecting evaluation, and exploration risk analysis in onshore, shallow, and deep water. His research interests are sedimentology, stratigraphy, and basin analysis.

Carlos Jorge de Abreu ~ *Instituto de Geociências, Universidade de Brasília, Brasília, Federal District, Brazil; joabreu@unb.br*

Carlos J. Abreu is a petroleum geologist at the Universidade de Brasília where he is presently teaching. He has an M.S. degree from Cincinnati University and a Ph.D. from Universidade Federal do Rio de Janeiro in Rio de Janeiro. He has worked for Petrobras for 24 years on projects concerned with the quality of siliciclastic reservoirs of petroliferous Brazilian sedimentary basins. He was the AAPG regional Latin America president in 2003–2005.

Frederico Antonio Genezini ~ *Instituto de Pesquisas Energéticas e Nucleares-Comissão Nacional de Energia Nuclear (IPEN-CNEN) São Paulo, Brazil; fredzini@ipen.br*

Frederico A. Genezini is a physicist with an M.S. degree and Ph.D. in nuclear technology. As a researcher in the Research Reactor Center at IPEN-CNEN, he works with the IEA-R1 research reactor on nuclear instrumentation and applied nuclear physics.

ACKNOWLEDGMENTS

The authors acknowledge Project POTI Agência Nacional do Petróleo, Gás Natural e Biocombustíveis–Universidade de Brasília–Parnaíba Gás Natura for financial support and Andrew Carter for dosimeter glasses. We are also thankful to Léo A. Hartmann for reviewing this manuscript. The first author thanks Coordenação de Aperfeiçoamento de Pessoal de Nível Superior within the Ministry of Education of Brazil for the student grant (PROSUC/88887.150578/2017-00).

INTRODUCTION

Petroleum systems occur in a variety of geological contexts and require several factors to generate and preserve hydrocarbons. Physical and thermochemical factors control conditions for hydrocarbon generation and accumulation. Physical factors of petroleum systems involve organic carbon matter accumulation, followed by hydrocarbon migration and retention under trapping and sealing conditions. The thermochemical factors are also important in the altering of rock properties, resulting in organic matter transformations through stages of hydrocarbon maturation. The maturation stages are achieved as a result of increasing temperature (e.g., burial and magmatic intrusion) during sedimentary basin evolution (Magoon and Dow, 1994; Welte et al., 2012).

Distinct types of sedimentary basins have thermal behaviors linked to their tectonic settings. During basin evolution, different tectonic events occur through extensional or compressional forces and result in basin subsidence or uplift. These events change thermal behavior by modifying the geothermal gradient of the upper crust (Allen and Allen, 2013). Usually, burial is the primary mechanism that increases temperature and contributes to hydrocarbon generation. In shallow basins, other processes are necessary to naturally achieve hydrocarbon maturation temperatures. Magoon and Dow (1994) describe these petroleum systems as atypical petroleum systems in which hydrocarbons are generated by means other than overburden. Intrusive magmatic activity is a prime example of a mechanism to form an atypical or unconventional petroleum system, as intrusion-triggered maturation type (de Miranda et al., 2018). Several actively explored petroleum systems are based on igneous intrusion models (e.g., Faroe Shetland Basin, North Atlantic and Gunnedah and Browse Basins, Australia; see more in Senger et al., 2017). Intrusions can also affect other petroleum system elements and processes (migration, reservoir, trap, and seal). The understanding of these thermal factors can lead to predictive models to target promising areas for hydrocarbon resources (Poelchau et al., 1997; Yalçin et al., 1997; Senger et al., 2017).

During the consolidation of Gondwana in the Paleozoic (e.g., Scotese et al., 1979), several sedimentary basins started to develop. In the western part of the supercontinent, the Parnaíba, Congo, Paraná, and Cape-Karoo Basins covered large areas and displayed similarities in their intracratonic origins and depositional histories (Linol et al., 2016). They each have complex postdepositional thermal histories associated with tectonic processes (Svensen et al., 2017). In the north, the basins had extensional movements, resulting in the opening of the Central and North Atlantic Ocean. These movements triggered subvolcanic magmatism collectively termed the Central Atlantic magmatic province (CAMP) (e.g., Marzoli et al., 1999; Mizusaki et al., 2002;

Nomade et al., 2007) that extensively intruded cratonic areas and sedimentary basins in the Jurassic and were recorded in thermochronological ages as shown by Dias et al. (2017) in the Araguaia Belt, Brazil. In the south, the extensional context led to the Paraná–Etendeka magmatism emplacement during the Cretaceous that thermally affected the Brazilian margin (e.g., Engelmann de Oliveira et al., 2016). Some of these magmatic events influenced the petroleum systems of the Paleozoic intracratonic basins of Gondwana and have been studied by Brown et al. (1994), Milani and Zalán (1999), Burke et al. (2003), Zalán (2004), and Thomaz Filho et al. (2008).

In the Parnaíba Basin, the magmatic activity affected rocks of the Upper Devonian–Carboniferous petroleum systems (Rodrigues, 1995). The basin has sedimentary layers (Mosquito and Sardinha Formations) that are nearly horizontal and continuous, which were intruded during the Mesozoic by two major magmatic events. These events are associated with the CAMP and Paraná–Etendeka magmatism and occur as sills and dykes between different sedimentary strata (Heilbron et al., 2018). Intrusions impacted thermal maturation of source rocks, migration enhancement, stratigraphic trapping, seals, and reservoir rocks. In these settings, the reservoir porosity and permeability were altered by intrusions and have irregular shapes, controlled by the placement and heat exchange with the igneous intrusions (Kingston and Matzko, 1995; Porto and Pereira, 2014; de Miranda et al., 2016, 2018).

The Parnaíba Basin is the fourth most productive basin for natural gas in Brazil (Agência Nacional do Petróleo, Gás Natural e Biocombustíveis, 2017). According to the Brazilian National Petroleum Agency, the gas production in the Parnaíba Basin in 2017 was approximately 5700 million m^3/day (~35,851 million bbl/day). Its main petroleum systems comprise the Pimenteiras Formation as principal source rock with total organic carbon values of 0.5–5 wt. %. Its organic matter was thermally matured by saucer-shaped igneous intrusions. The Poti and Cabeças Formations are the main reservoirs with average porosities of 18% and 13%, respectively (Cunha et al., 2012; de Miranda et al., 2018). The hydrocarbon migration model from the Pimenteiras source rock to Cabeças and Poti reservoirs includes migration by stratigraphic contact, and through faults from Permian to Middle Jurassic and Lower Cretaceous (Agência Nacional do Petróleo, Gás Natural e Biocombustíveis, 2015). In the case of the reservoir rocks closely placed to igneous bodies, hornfel aureoles are common and can thermally eliminate the reservoir quality of sandstones. This petroleum system is directly associated with the magmatic intrusions that also acted as stratigraphic and structural traps (Rodrigues, 1995; Agência Nacional do Petróleo, Gás Natural e Biocombustíveis, 2015).

Application of apatite fission-track (AFT) and zircon fission-track (ZFT) analyses in hydrocarbon exploration are well-established methods that allow paleotemperature determination in ranges of approximately 60°C–120°C and 180°C–320°C, respectively (e.g., Bernet and Garver, 2005; Donelick et al., 2005). These analyses are widely used to constrain the thermal history of the upper crust and provide constraints on the timing and duration of heating and cooling events in sedimentary basins (e.g., Green et al., 2004; Engelmann de Oliveira et al., 2016). The ZFT method is particularly useful in the Parnaíba Basin because the temperature range is comparable to the gas maturation stage (>200°C).

In this study, an integrated approach combining petrography, AFT, and ZFT analyses was applied to gain an understanding of the influence of igneous rocks on obtaining the maximum paleotemperatures and qualities of potential reservoir rocks in the eastern part of the Parnaíba Basin. For this purpose, outcrop and borehole samples were analyzed to constrain the thermal history of the rocks and to provide evidence for high-temperature alteration of the reservoir rocks.

GEOLOGICAL SETTING

The Parnaíba Basin is an intracratonic sedimentary basin that covers approximately 600,000 km^2 (~232,000 mi^2) of northeastern Brazil (Figure 1A, B) and has a 3.5-km (11,500-ft)-thick volcanic-sedimentary record (Figure 1C, D) with a long Phanerozoic depositional history (e.g., Góes and Feijó, 1994; Vaz et al., 2007). The basin covers an amalgamation of different Precambrian terranes generated during the Brasiliano orogeny (de Brito Neves, 2002). Basement rocks of the basin are divided into (1) the Parnaíba block in a totally covered central area showing featureless reflector patterns and interpreted as granitic terrane (Daly et al., 2014) and (2) basin edges partially covering cratonic areas (Amazonas, São Luís, and São Francisco cratons) and mobile belts (Gurupi Belt, and Borborema

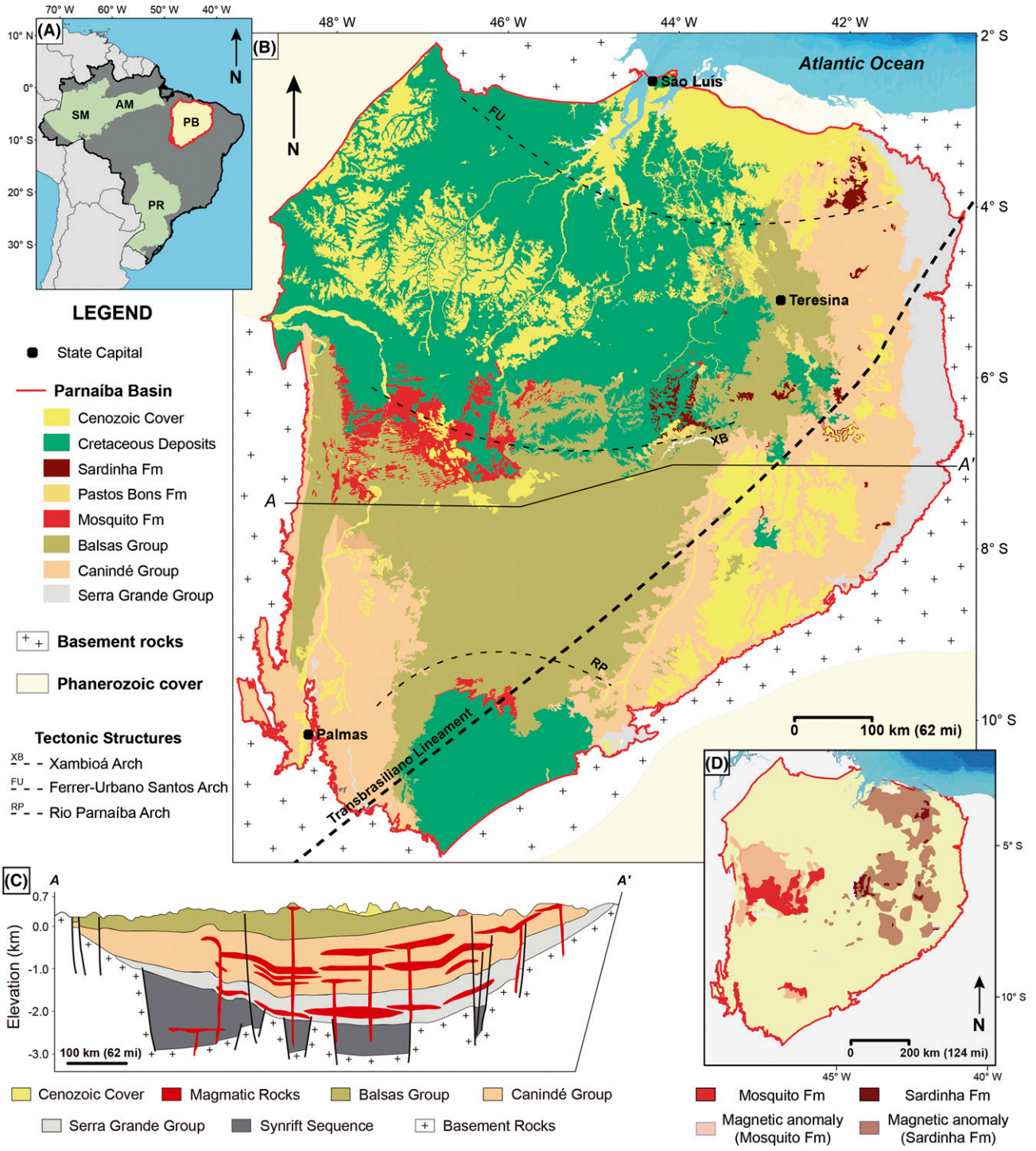

Figure 1. (A) Location map. Brazilian Paleozoic intracratonic basins. (B) Parnaíba Basin divided in sedimentary units and major tectonic structures. (C) Schematic cross section of the Parnaíba Basin (modified from Góes et al., 1990). (D) Interpretative geophysical map of the magnetic anomalies of the Mosquito Formation (Fm) and the Sardinha Fm (modified from Mocitaiba et al., 2017). AM = Amazonas Basin; PB = Parnaíba Basin; PR = Paraná Basin; SM = Solimões Basin.

and Tocantins provinces), which are distinct blocks and suture zones juxtaposed during the Brasiliano orogeny (de Castro et al., 2014).

During the early Cambrian–Ordovician, lithospheric stretching of western Gondwana and Laurentia resulted in the reactivation of a rift system along preexisting basement weakness. The extension formed northeast to east-west–oriented grabens along the Transbrasiliano lineament, such as the Jaibaras trough (de Oliveira and Mohriak, 2003). These early Paleozoic grabens were filled by fluvial–lacustrine sediments of the presag stage of the Parnaíba Basin (Almeida and Carneiro, 2004). The initial subsidence of the late Parnaíba Basin sag stage is a result of thermal subsidence (lithospheric contraction) during the Ordovician–Silurian. From initial subsidence until the Mississippian, the principal depositional axis of the basin was over the Transbrasiliano lineament on the eastern edge (de Oliveira and Mohriak, 2003; Daly et al., 2014; de Castro et al., 2016).

The sedimentary infill of the Parnaíba Basin is divided into five supersequences bounded by major unconformities (Figure 2A): Silurian, Middle Devonian–Mississippian, Pennsylvanian–Lower Triassic, Jurassic, and Cretaceous (i.e., Vaz et al., 2007). The Silurian supersequence corresponds to a second-order transgressive–regressive cycle. It covers the basement and includes sandstones and siltstones. This supersequence corresponds to the Serra Grande Group described by Della Fávera (1990), Góes and Feijó (1994), and Góes (1995).

The Middle Devonian–Mississippian supersequence lies above the Silurian supersequence and is equivalent to the Canindé Group. The group includes sandstones and mudstones of the Itaim, Pimenteiras, Cabeças, Longá, and Poti Formations. The Itaim Formation is described as a shallow marine, storm-dominated sandstone. The Pimenteiras Formation is characterized by fine-grained rocks and includes organic-rich black shales, which correspond to the maximum flooding stage of this supersequence as well as the entire depositional history of the Parnaíba Basin (Vaz et al., 2007). The Cabeças Formation comprises glacially influenced, shallow marine sandstones. The Longá Formation includes sandstone and siltstone deposited under similar conditions to the Itaim Formation. In addition, the uppermost Poti Formation includes sandstones related to transitional environments (upper shoreface, estuarine, and fluvial–estuarine) (Góes and Feijó, 1994; Góes, 1995; Milani and Zalán, 1999; Vaz et al., 2007).

In the Pennsylvanian, Pangea assembling started to compress and uplift some areas such as the Ferrer-Urbano, Santos, and Rio Parnaíba arches, moving the basin depocenter toward the west (Xambioa arch; Figure 1) and delimiting the contour of the Parnaíba Basin. The Pennsylvanian–Lower Triassic supersequence is related to a drastic climate change that took place when open seas of temperate climate became restricted because of global sea-level fall (Becker, 1993). During this period, a progressive desertification occurred in the basin with deposition occurring under arid conditions. This supersequence is also called the Balsas Group and was dominated by continental and restricted marine depositional settings (e.g., Araújo et al., 2016; Vieira and Scherer, 2017). Extensional movements related to Pangea rupturing caused the intrusion of sills and dykes of Jurassic (Mosquito Formation) and Cretaceous age (Sardinha Formation) (Figure 1C, D) (Fodor et al., 1990; Silva et al., 2017).

The Mosquito Formation comprises basaltic dykes and sills associated with the early North and Central Atlantic Ocean rift (ca. 200 Ma) (Merle et al., 2011) and Penatecaua magmatism in the Amazonas Basin as part of CAMP (Marzoli et al., 1999). The Jurassic supersequence is formed by the Pastos Bons Formation, whose sediments were deposited in continental environments in low areas because of magmatic overburden of the Mosquito Formation.

During the Cretaceous, the South Atlantic Ocean rift caused major marine transgressions changing depositional systems. Rifting movements along with west Gondwana continental break-up generated new intrusions, such as the Sardinha Formation, that were formed by dykes of Early Cretaceous age (120–130 Ma) (Fodor et al., 1990; Baksi and Archibald, 1997) and associated with magmatism of the Serra Geral Group in the Paraná Basin (Thomaz Filho et al., 2000). The final supersequence is Cretaceous, deposited in continental–transitional marine environments (aeolian and fluvial–lacustrine to shallow platform) with the depocenter located in the northwestern part of the basin, and composed of the Corda, Grajaú, Codó, and Itapecuru Formations.

MATERIALS AND METHODS

Samples from four outcrops and the Bom Princípio/Piauí (BPP) borehole (six samples) were collected in

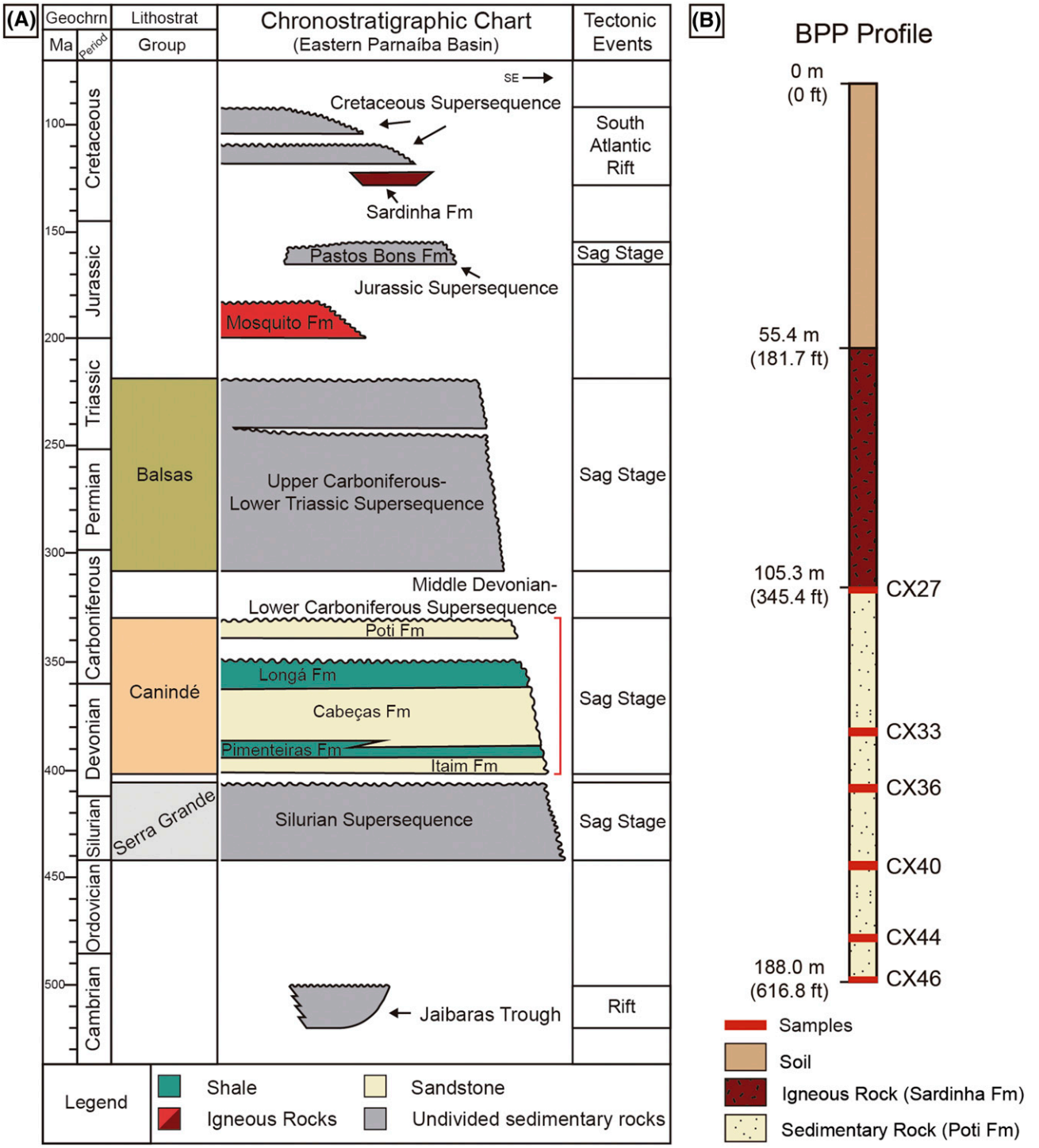

Figure 2. (A) Chronostratigraphic chart of eastern Parnaíba Basin (modified from Vaz et al., 2007). (B) Schematic profile of Bom Princípio/Piauí (BPP) borehole. Red marks highlight position of collected samples. CX = borehole caixa (box) sample; Geochrn = geochronology; Fm = Formation; Lithostrat = lithostratigraphy.

Table 1. Details of Samples Studied with Fission-Track and Petrography

Lithology/Formation	Sample	Latitude	Longitude	Elevation/ Depth, m	Elevation/ Depth, ft	Stratigraphic Age, Ma	AFT	ZFT	Petrography
Borehole BPP									
Sandstone/Poti	CX27	42° 19′ 22″	06° 30′ 07″	– / 105.3–106.3	– / 345.5–348.7	331–339	X	X	X
Sandstone/Poti	CX33	42° 19′ 22″	06° 30′ 07″	– / 134.9–136.3	– / 442.5–447.2	331–339	X	X	X
Sandstone/Poti	CX36	42° 19′ 22″	06° 30′ 07″	– / 146.9–148.3	– / 481.9–486.5	331–339	X	X	X
Sandstone/Poti	CX40	42° 19′ 22″	06° 30′ 07″	– / 163.0–164.5	– / 534.8–539.7	331–339	X	X	X
Sandstone/Poti	CX44	42° 19′ 22″	06° 30′ 07″	– / 178.2–179.5	– / 584.6–588.9	331–339	X	X	X
Sandstone/Poti	CX46	42° 19′ 22″	06° 30′ 07″	– / 187.1–188.0	– / 613.8–616.8	331–339	X	X	X
Outcrop									
Sandstone/Corda	PA02B	42° 57′ 12″	06° 48′ 08″	135 / –	443 / –	111–119	X	X	X
Siltstone/Pastos Bons	PA03A	42° 57′ 06″	06° 48′ 30″	146 / –	479 / –	154–165	X	X	X
Siltstone/Poti	PA06	43° 11′ 26″	06° 42′ 18″	121 / –	397 / –	331–339		X	
Sandstone/Cabeças	PA09A	41° 34′ 34″	07° 01′ 58″	274 / –	899 / –	364–390	X	X	X

Abbreviations: – = none; AFT = apatite fission track; BPP = Bom Princípio/Piauí; CX = borehole caixa (box) sample; PA = Parnaíba Basin outcrop sample; X = method applied according to sample; ZFT = zircon fission track.

the Parnaíba Basin from the Cabeças, Poti, Pastos Bons, and Corda Formations in areas near intrusive bodies (<40 m [<131 ft], except sample PA06). More details of each sample are provided in Table 1 and Figures 2B and 3.

Petrography

Petrographic analysis was performed on three outcrop samples and all six borehole samples. These samples were selected to study petrographic aspects of the interaction between intrusions and sedimentary rocks, and because they integrate reservoir layers within the thermal influence zones of the igneous bodies showing thermal alteration textures. The depositional and diagenetic study included thin sections of samples under the optical polarizing microscope Zeiss AXIO Lab.A1 with 2.5×, 10×, 20×, and 50× objectives at Universidade do Vale do Rio dos Sinos, Brazil. Petrographic information can be found in Tables 2 and 3. Standard point-counting techniques (Dickinson et al., 1983) were used to distinguish different components of the sedimentary rocks.

Thermochronology

The basic principles of thermochronology of fission-track dating have been extensively reviewed by several authors (e.g., Wagner and Van den haute, 1992; Tagami and O'Sullivan, 2005; Carter, 2007; Gleadow and Seiler, 2015). Fission tracks are stable over geological time only at relatively low, near-surface temperatures (Armstrong, 2005). As the temperature is raised, the radiation damage is progressively repaired until the track no longer forms a continuous defect that can be revealed by etching. This process of fission track fading upon exposure to elevated temperatures is called annealing. Annealing is a kinetic process in which temperature and time can, to some extent, be interchanged. Longer exposure to lower temperatures can produce the same effect as shorter exposure to higher temperatures. Each mineral shows a different characteristic temperature range over which fission-track annealing occurs, commonly referred to as the partial annealing zone (PAZ). For apatite, this annealing range is approximately 60°C–120°C, with significantly higher characteristic annealing temperatures of approximately 180°C–320°C for zircon.

The AFT and ZFT thermochronology were performed on all samples (Table 1). Apatite and zircon grains were concentrated using conventional methods of crushing and magnetic, heavy liquid and hand-picking separation. Apatite grains were mounted in epoxy resin and polished and etched for 20 s in a 5.5 M HNO_3 solution at 21°C to reveal the fission tracks. Zircon grains were mounted in Teflon

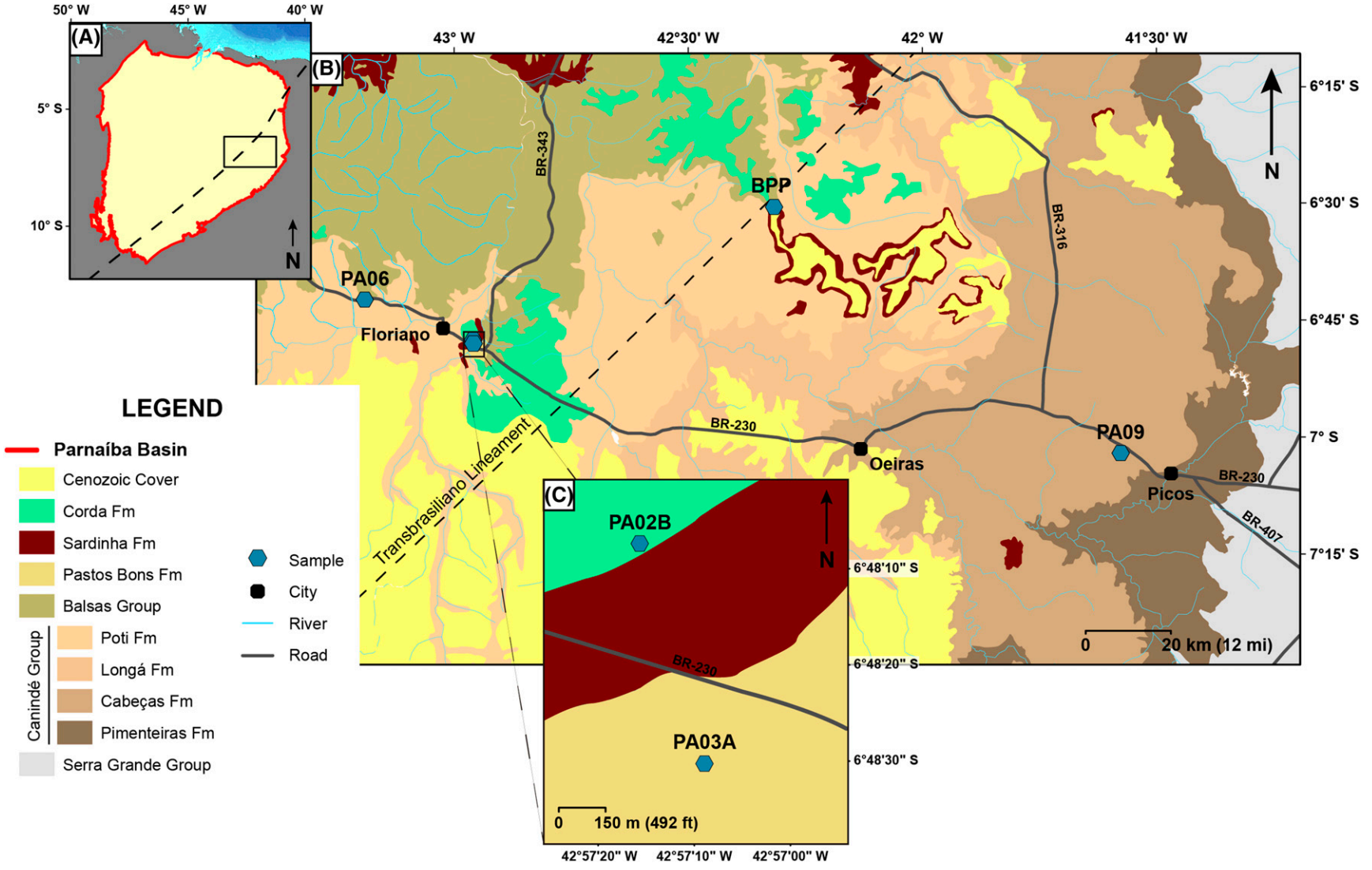

Figure 3. Geologic map of the study area. (A) Parnaíba Basin and the Transbrasiliano lineament. (B) Study area. Borehole Bom Princípio/Piauí (BPP) and sample location. (C) Location of samples PA02B and PA03A. BR = federal road naming convention; Fm = Formation; PA = Parnaíba Basin outcrop sample.

Table 2. Modal Composition

Sample	Monoquartz/Polyquartz	Feldspar	Rock Fragments	Cement	Porosity	Others	Total
Poti Formation							
CX27	58/13	1	1	18	9	–	100
CX33	50/12	1	3	15	19	–	100
CX36	57/17	3	–	10	12	1	100
CX40	61/15	7	1	4	2	5	100
CX44	62/13	8	2	9	3	3	100
CX46	52/18	9	1	14	5	1	100
Corda Formation							
PA02B	50/8	8	2	14	17	1	100
Cabeças Formation							
PA09A	50/9	–	1	12	28	–	100

Results are in percent based on point counting in each sample. Feldspar includes K-feldspar and plagioclase. Cement is kaolinite, quartz, or ferruginous minerals. Porosity is secondary. Other minerals are zircon, mica, and Fe-oxides.
Abbreviations: – = none; CX = borehole caixa (box) sample; PA = Parnaíba Basin outcrop sample.

PFA and polished and etched in a NaOH-KOH melt solution at 230°C. The multimount technique was adopted, and two or three zircon mounts were prepared per sample (Bernet and Garver, 2005) and etched for different periods of time ranging from 3 to 14 hr. The mounts were covered with low-U mica sheets and dated by the external detector method (Hurford, 1990). Neutron irradiation was done in the IPEN-CNEN Reactor, São Paulo, Brazil, using uranium-doped silicate dosimeter glasses, Durango age standard for apatite mounts, and Fish Canyon Tuff age standard for zircon mounts.

The AFT and ZFT analyses were performed at the Low-Temperature Thermochronology Lab at Universidade de São Paulo, Brazil, using an Olympus BX51 Microscope (1250×, dry) with a digitalizing tablet and a computer-controlled stage driven by the FTStage 4.05 software (Dumitru, 1993). A summary of AFT and ZFT data is presented in Table 4. The AFT and ZFT ages and errors were calculated following the zeta-calibration method (Hurford and Green, 1983) with the RadialPlotter software (Vermeesch, 2009). Fission-track age errors are quoted at 1σ confidence level and derived by conventional

Table 3. Selected Petrographic Information

Sample	Average Size, mm	Sorting	Rounding	Sphericity	Compaction Grain Contacts	Matrix
Poti Formation						
CX27	0.7/0.3	Moderate	Subrounded to rounded	Low	Long	None
CX33	1.5/0.2	Moderate	Subrounded to rounded	Low	Long	None
CX36	1/0.5	Moderate	Subrounded to rounded	Low	Long	None
CX40	0.3	Well	Subrounded to rounded	High	Long	None
CX44	0.3	Well	Subrounded to rounded	High	Long	None
CX46	0.2	Well	Subrounded to rounded	High	Long	None
Corda Formation						
PA02B	0.3	Well	Subrounded	Low	Long	None
Pastos Bons Formation						
PA03A	>0.1	Well	Rounded	High	–	Fe-oxides
Cabeças Formation						
PA09A	0.5	Moderate	Subangular to subrounded	Low	Point to long	None

All information was visually determined in the majority of grains and contacts in thin sections during point counting.
Abbreviations: – = none; CX = borehole caixa (box) sample; PA = Parnaíba Basin outcrop sample.

Table 4. Apatite and Zircon Fission-Track Data

Sample	Dating Method	Etching Time, hr	*N*	ρs, $\times 10^5$	*Ns*	ρi, $\times 10^5$	*Ni*	ρd, $\times 10^5$	*Nd*	Central Age, Ma	$\pm 1\sigma$, Ma	χ^2, %	*U*, ppm	*Dpar*, μm	*n*	MTL, μm	S.D., μm	Group I Age, Ma (%)	Group II Age, Ma (%)
Borehole BPP																			
CX27	ZFT	5	39	73.3	3901	8.7	466	1.6	2500	92.8	9.3	0	194.7	–	–	–	–	57 (45)	172 (55)
CX33	AFT		22	0.5	67	1.0	125	19.7	6001	24.2	8.9	0	2.0	–	–	–	–	16 (92)	186 (8)
	ZFT	3–8	39	116.1	5695	5.2	253	1.6	2500	210.0	25.0	0	114.7	–	–	–	–	80 (16)	298 (84)
CX36	ZFT	3–8	49	97.1	4777	5.3	259	1.6	2500	182.0	23.0	0	117.1	–	–	–	–	92 (26)	291 (74)
CX40	AFT		31	0.2	22	0.7	90	19.7	6001	20.4	7.8	3	1.3	–	–	–	–	7 (82)	140 (18)
	ZFT	5–6	51	157.9	4909	3.0	92	1.6	2500	563.0	59.0	100	65.8	–	–	–	–	–	–
CX44	AFT		51	0.3	90	0.5	177	19.7	6001	67.0	8.7	78	1.0	–	–	–	–	–	–
	ZFT	3–9	31	134.0	3941	2.4	71	1.6	2500	576.0	76.0	36	53.7	–	–	–	–	–	–
CX46	ZFT	3–10	49	108.9	5244	3.6	172	1.6	2500	324.0	27.0	19	79.5	–	–	–	–	–	–
Outcrop																			
PA02B	AFT		50	0.1	28	0.3	91	19.7	6001	34.0	8.6	84	0.6	1.3	5	10.3	2.1	–	–
	ZFT	3–8	46	54.1	3229	8.2	487	1.6	2500	72.6	4.1	9	181.4	–	–	–	–	–	–
PA03A	AFT		18	1.7	92	1.2	64	19.7	6001	130.0	31.0	7	2.2	2.4	19	11.3	1.6	–	–
	ZFT	4–14	03	80.3	257	4.1	13	1.6	2500	215.0	61.0	36	90.4	–	–	–	–	–	–
PA06	ZFT	7	16	125.5	1310	2.7	28	1.6	2500	497.0	95.0	58	59.7	–	–	–	–	–	–
PA09A	ZFT	3–11	40	124.8	4963	3.0	118	1.6	2500	447.0	43.0	23	66.0	–	–	–	–	–	–

Apatite fission-track (AFT) age calculated using C. Engelmann de Oliveira zeta-calibration, ζ-CN2 – 135.4. Calibration parameters: *aLen* = 1.45 and *aDpar* = 0.60.

Abbreviations: – = none; 1σ = standard deviation; $\chi 2$ = chi-square probability; ρi = measured induced track density; ρd = track density measured in glass dosimeter; ρs = measured spontaneous track density; *aLen* = calibration parameter value; BPP = Bom Princípio/Piauí; CX = borehole caixa (box) sample; *Dpar* = mean etch pit diameter of all measured etch pits; MTL = mean track length; *n* = number of confined track lengths measured; *N* = number of grains analyzed to determine track densities; *Nd* = number of tracks counted in determining ρd; *Ni* = number of induced tracks counted; *Ns* = number of spontaneous tracks counted; PA = Parnaíba Basin outcrop sample; S.D. = standard deviation of track length distribution of individual track measurements; *U* = calculated uranium content; ZFT = zircon fission track.

method (Green, 1981). The chi-square test (χ^2) was used to quantify individual ages of a unique population, in which $\chi^2 > 5\%$ is considered to represent a concordant age so samples contain a single age population (Galbraith and Laslett, 1993). The AFT lengths were measured on horizontal confined fission tracks. Etch pit diameter (*Dpar*) values were used as a kinetic parameter. The *Dpar* value is the arithmetic mean fission-track etch figure diameter parallel to the crystallographic c-axis and is positively correlated with Cl wt. % (Donelick et al., 2005).

Thermal modeling was performed using the HeFTy version 1.9.3 software (Ketcham, 2005). The input data include AFT and ZFT ages, track lengths when available, and *Dpar* as a kinetic parameter. The kinetic annealing model of Ketcham et al. (2007) was used for AFT and Rahn et al. (2004) for ZFT. The inversion modeling was run until 100 good models (goodness of fit > 0.5) were obtained (Ketcham, 2005) using a Monte-Carlo search method. Stratigraphic ages and present-day temperature were included as constraints, allowing the software to search for a wide range of a coherent time–temperature spectra. Additional constraining boxes delimitate the intrusion age of the Mosquito and Sardinha Formations; ages of the youngest unconformities of the basin (125–120 and 110–105 Ma) were included for thermal modeling of the samples.

RESULTS

Petrography

Poti Formation samples from the borehole (caixa [CX], meaning box samples) are mostly composed of mono- and polycrystalline quartz (>85 vol.%); plagioclase and K-feldspar are present in minor proportions (Table 2) and rock fragments are rare. Using the Dickinson et al. (1983) diagram, these samples are derived from intracratonic sources (Figure 4). Samples are subarkose sandstones, grain-supported with long compaction contacts between grains. Other petrographic information can be found in Table 3. In the borehole samples, two major groups show different depositional and diagenetic features. The upper group (CX27, CX33, and CX36; Figure 5A–C) has bimodal grain distribution of two average grain sizes in thin section. The lower group (CX40, CX44, and CX46; Figure 5D–F) has smaller grain size and higher sphericity compared to the upper group.

The upper group is cemented by kaolinite and chalcedony. Grain dissolution resulted from eodiagenesis (Figure 5A). The lower group has similar cement in the pore spaces but different diagenetic composition. Illitic clays (illite and smectite) formed from micas. Small, nearly cubic crystals of pyrite are present (Figure 5D).

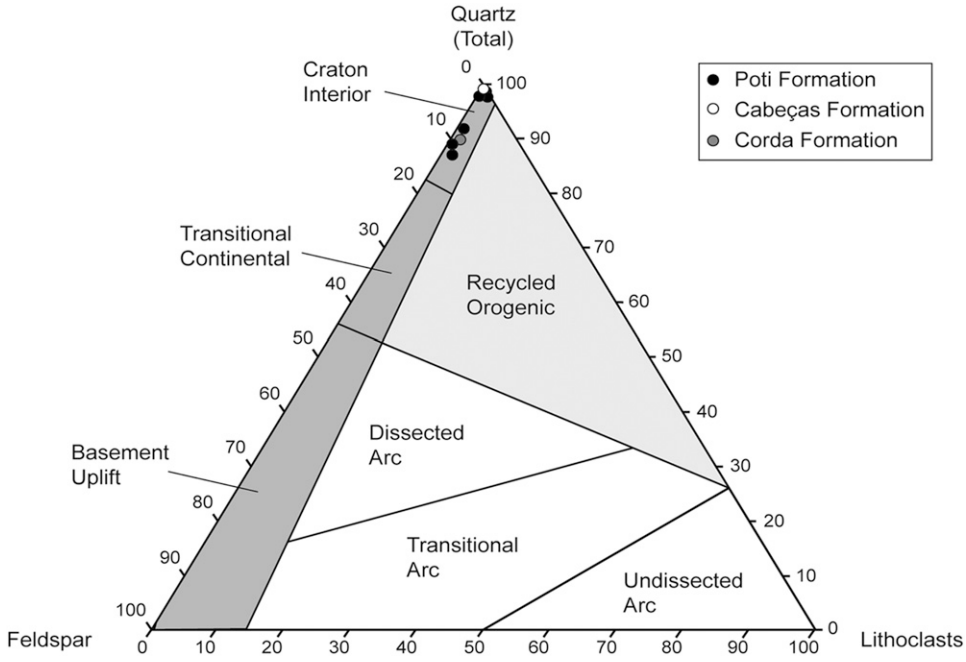

Figure 4. Sandstone provenance diagram (Dickinson et al., 1983) indicates quartzose rocks from craton interior sources.

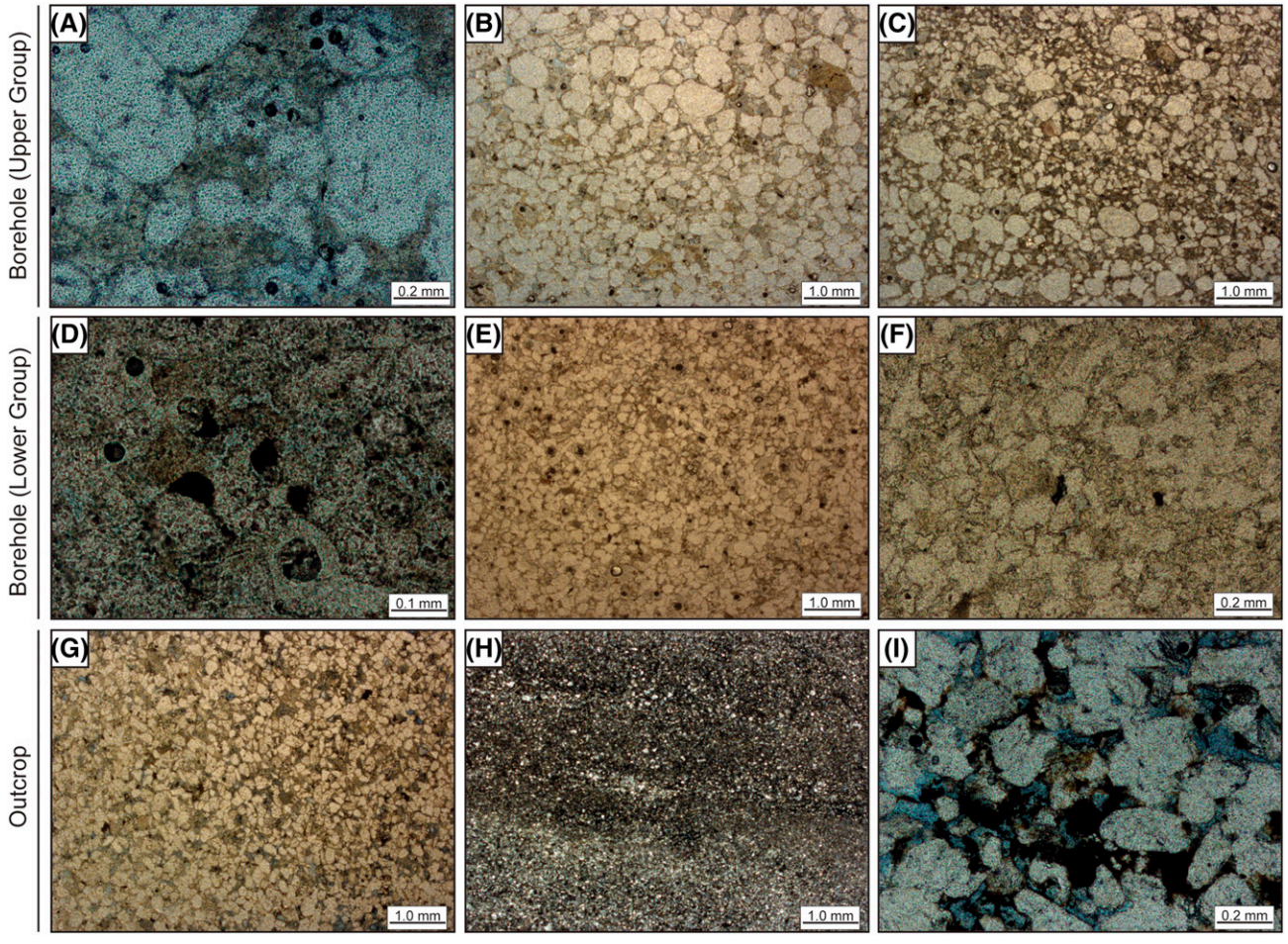

Figure 5. (A) Dissolution features in sample CX27 in natural light (NL) (×10). (B) Pore space filling by carbonate cement in sample CX33 in NL (×2.5). (C) Bimodal grain-size distribution in sample CX36 in NL (×2.5). (D) Pyrite crystals inside pores in sample CX40 in NL (×20). (E) Small grain size in sample CX44 in NL (×2.5). (F) Tightly packed texture with little pore space in sample CX46 in NL (×10). (G) Pyrite crystals (black spots) in pore space of sample PA02B in NL (×2.5). (H) Siltstone with bioturbation structures in sample PA03A in NL (×2.5). (I) Black to red ferruginous cement (hematite and goethite) in sample PA09A in LN (×10). CX = borehole caixa (box) sample; PA = Parnaíba Basin outcrop sample.

Porosity differentiates the two groups, but primary porosity was not found in any sample. Primary porosity was occluded as a result of compaction and postdepositional cementation (Figure 5B). Following standard 300-point counting, samples showed secondary porosity from grain and cement dissolution. In the borehole samples, the upper group has higher porosity than the lower group (Figure 5B, F).

Sample PA02B from the Corda Formation shows distinct petrographic characteristics compared to CX samples. Grains are subrounded and well sorted. Compared to other sandstones, PA02B has higher porosity and cement in pore space. Cementation is similar to the lower group from Poti samples with initial illitic clay formation and occurrence of pyrite crystals (Figure 5G). A sample from the Pastos Bons Formation (PA03A) is a siltstone composed of quartz and mica. The sample shows a reddish ferruginous cementation (hematite and goethite). The principal features in this sample are the trace fossil structures along with pyrite (Figure 5H).

The Cabeças Formation sample (PA09A) shows a moderately sorted sand-size framework composed mostly of mono- and polycrystalline quartz (>95%). Grains of plagioclase and K-feldspar occur, and rock fragments are rare. The sample has medium-point to long-compaction grain contacts. The porosity percentage is higher than the other samples, and cementation is made of ferruginous minerals (hematite/goethite) and kaolinite (Figure 5I).

Thermochronology

The AFT and ZFT results are presented in Table 4. The ZFT age distribution is shown in Figure 6. Thermal history models are presented in Figures 7 and 8.

Apatite Fission-Track Data

The AFT data from borehole and outcrop samples have central ages ranging from 20.4 ± 7.8 to 130 ± 31 Ma. Samples CX33 and CX40 have low χ^2-test values, indicating more than one age population. Apatite grains from sedimentary rocks show high PAZ resetting with little or even no spontaneous fission tracks. Nonetheless, induced fission tracks in all apatite samples support an AFT central age much younger than ZFT central ages of correlating samples (Table 4).

Among borehole samples, CX33 shows two-age distributions with a higher proportion of a younger age of 16.8 ± 6.1 Ma (92%) compared to the older 186 ± 41 Ma (8%). Sample CX40 shows a similar two-age distribution of 7.7 ± 8 Ma (82%) and 140 ± 79 Ma (18%). In a lower position, CX44 recorded an average central age of 67 ± 8.7 Ma. In outcrop samples, PA02B shows a central age of 34 ± 8.6 Ma and a mean track length (MTL) of 8.92 ± 1.01 μm, and sample PA03A recorded an average central age of 130 ± 31 Ma and an MTL of 9.28 ± 0.79 μm. For these samples, measured *Dpar* values range from 2.36 μm for PA03A to 1.28 μm for PA02B.

Zircon Fission-Track Data

The ZFT central ages range from 72.6 to 576.0 Ma (Figure 6; Table 4). Zircon grains have U-concentrations of 53.7–194.7 ppm (Table 4). Three samples have low χ^2-test values, indicating more than one age population in the ZFT analyses. The uppermost sample, CX27, shows two ages, one at 57.3 ± 4.2 Ma (45%) and an older at 172 ± 17 Ma (55%). Almost 29 m (95 ft) downward in the core, sample CX33 also shows two ages (80 ± 15 and 298 ± 27 Ma) but with more grains from the older population (16% and 84%). Sample CX36 is located 10 m (33 ft) below CX33 and presents two ages, one at 92 ± 15 Ma (26%) and an older at 291 ± 34 Ma (74%). Stratigraphically below the three upper samples, CX40 shows a central age of 563 ± 59 Ma and CX44 an age of 576 ± 76 Ma. Both samples lack single grain ages younger than 185 Ma. The lowermost sample, CX46, records a central age of 324 ± 27 Ma with a few single grain ages as low as 112 Ma.

Central age distributions in outcrop samples vary similar to the borehole. Sample PA02B shows a young central age of 72.6 ± 4.1 Ma, whereas the Pastos Bons Formation sample (PA03A) records an older central age of 215 ± 61 Ma. Both samples are located close to an igneous intrusion (PA02A). Nevertheless, PA03A has fewer single grain ages, which enhances the error. A Poti Formation sample (PA06) shows a central age of 497 ± 95 Ma and the Cabeças Formation sample (PA09A) an age of 447 ± 43 Ma.

Thermal History Models

Based on fission-track parameters and geological background of the area, inversion models for the samples were developed using predefined constraints (Figure 7). The best-fit thermal models from borehole samples show maximum postdepositional paleotemperatures decreasing with depth and all occurring from circa 102 to 201 Ma. Sample CX27 shows good fitting paths with an initial constant heating reaching beyond the apatite PAZ with a maximum paleotemperature of approximately 367°C at 102 Ma, then a rapid cooling to present-day temperature. Likewise, samples CX33 and CX36 show increasing paleotemperatures until 130 and 136 Ma, when maximum paleotemperatures of 308°C and 313°C were reached, respectively, followed by a final cooling event to present-day temperature.

Borehole samples CX40 and CX44 show a predepositional thermal history with a recorded maximum paleotemperature at circa 600 to 560 Ma. After deposition, the rocks experienced a heating phase, in which the samples reached maximum paleotemperatures of approximately 149°C and 143°C at 133 and 155 Ma, respectively. Good fitting paths of sample CX46 record heating to a maximum temperature of approximately 123°C at 201 Ma, followed by a cooling event to present-day temperature.

Good fitting paths of sample PA03A show postdepositional heating to a maximum paleotemperature of approximately 72°C at 108 Ma and, thereafter, a cooling phase until present-day temperature. The best-fit thermal model from sample PA02B shows a sudden heating during deposition time to a maximum paleotemperature of approximately 355°C,

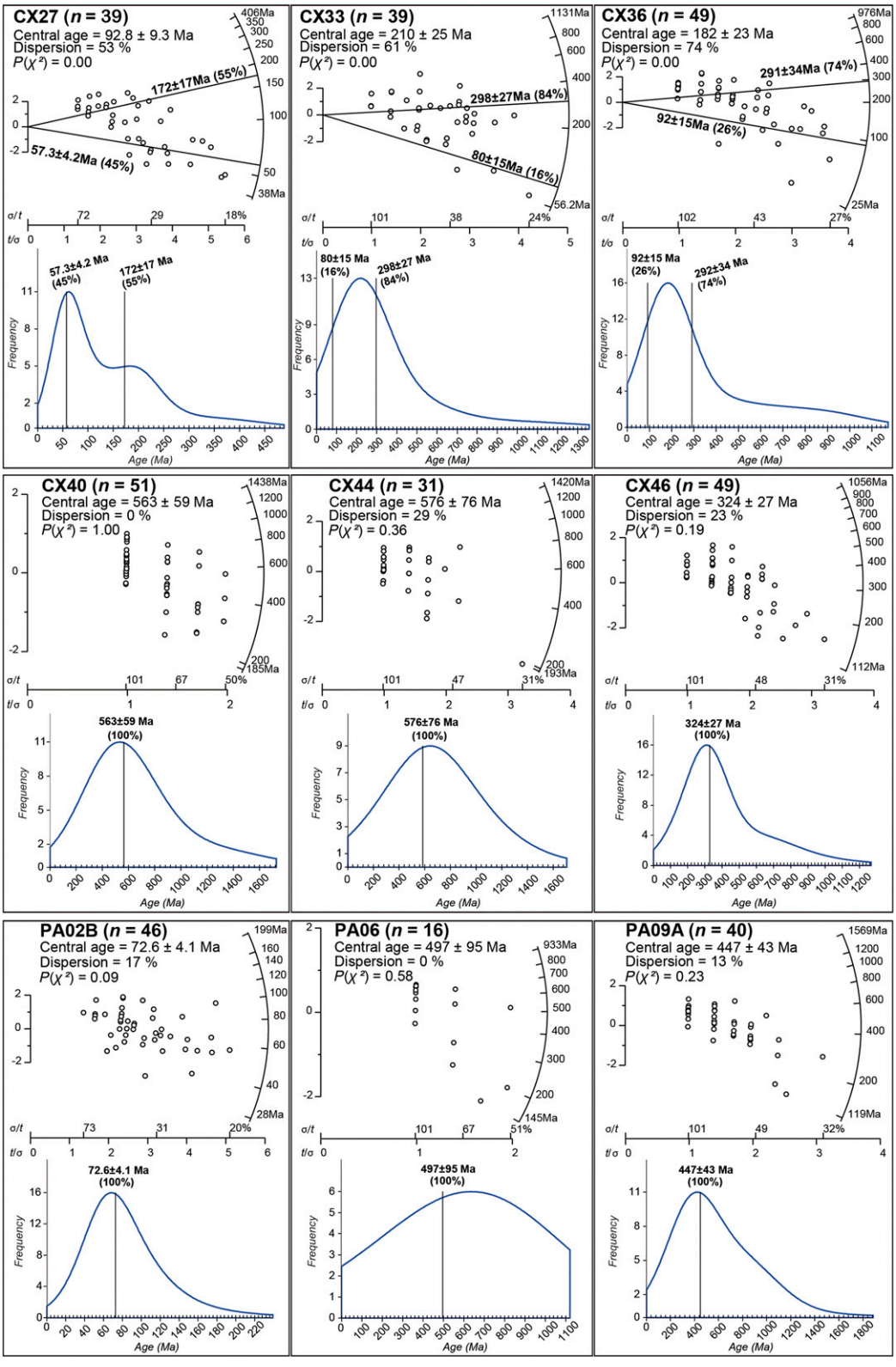

Figure 6. Radial plot diagrams and histograms with probability density of ZFT ages samples showing number of grains (*n*), central ages, dispersion, and chi-square (χ^2) test result. Each point has a unit of standard error in *y*-axis, a relative standard error (%), and precision in *x*-axis and age in the circular axis. σ = corresponding measurement uncertainty of the data; *P* = *P* value of a χ^2 probability for homogeneity of the samples; CX = caixa (box) sample; PA = Parnaíba Basin outcrop sample.

then a rapid cooling to apatite PAZ temperature, and thereafter to present-day temperature (Figure 8).

DISCUSSION

Dimension of the Thermal Effect on Potential Reservoir Rocks

Borehole samples are separated into two groups (upper and lower) by depositional and diagenetic properties, and the groups also reflect the thermochronology data that record a diverse thermal history. All AFT ages are much younger than depositional age and indicate a partial or total reset related to elevated temperature (above apatite PAZ) from the nearby igneous intrusion. In contrast, ZFT central ages record pre- and postdepositional ages. Postdepositional ages indicate a thermal influence of the two magmatic events, although the last event (Sardinha Formation) is better evidenced in the samples that show a clear division between the two groups in terms of maximum paleotemperature.

Comparing petrographic characteristics, the upper group (CX27, CX33, and CX36) shows larger, less spherical, and moderately sorted grains, implying less transport and reworking than the lower group (CX40, CX44, and CX46), which is composed of smaller and more spherical grains. The lower group also has mica sheets between quartz grains, implying a low-energy system compared to the upper group. Stages of eodiagenesis in all samples show precipitation of kaolinite inside pore spaces. Pores are also filled with quartz cement (chalcedony) overgrowing quartz grains. Compaction grain contacts emphasize that the samples were compacted enough to rearrange the grains and decrease the primary porosity when mechanical compaction started. The presence of secondary porosity by grain dissolution is linked to the high-temperature fluid percolation from the later intrusion of igneous rocks of the Mosquito and Sardinha Formations. This intragranular porosity was then filled with quartz cement and kaolinite from quartz and feldspar dissolution. The dissolution of detrital K-feldspar grains implies temperatures of approximately 50°C–150°C (Wilkinson et al., 2001) with the replacement by authigenic clay minerals (kaolinite) occurring at approximately 50°C–150°C (e.g., Wilkinson et al., 2001; Verdel et al., 2012). The correlation of porosity with average grain size shows that fewer pore spaces in the lower group probably result from major compaction of smaller grains. In contrast, the upper group shows a higher intragranular porosity possibly because of the larger grains and the hydrothermal influence of the intrusion (Houseknecht, 1988).

In terms of thermochronology, the upper group is positioned below the igneous sill and shows that it was highly influenced by the intrusion as demonstrated by the increase in older ZFT ages with depth until sample CX36 (Figure 6). The results of sample ages show a clear reduction in thermal effects with depth. Furthermore, in terms of maximum paleotemperature, inversion models of the upper group samples show influence up to sample CX36, in which samples underwent temperatures from approximately 367°C in CX27 to 313°C in CX36, correlated to the Sardinha Formation intrusion event (Figure 9). These paleotemperatures are similar to those found by Rodrigues (1995) using vitrinite reflectance in a different area of the basin. Although the intrusion affected all samples, the results also show a significant decay in thermal influence between samples CX36 and CX40 (~313°C–149°C), which corresponds to the limit of the intrusion influence. Therefore, the high temperature influence (>225°C) is verified up to approximately 51 m (~167 ft) from the intrusion contact with the sedimentary rocks (Figure 9). This distance is comparable to the influence described by Rodrigues (1995) of 0.8–1.3 times the size of the igneous body. However, it is not possible to make a correlation with the size of the igneous body because the intrusion is eroded at the top of the section. The high temperature (above the apatite PAZ) experienced by all apatite samples from the borehole is verified by the high degree of PAZ of the spontaneous fission tracks.

The lower group, approximately 60 m (~197 ft) from the intrusion (Figure 9), shows predepositional ZFT central ages ranging from 560 to 600 Ma, correlating to the Brasiliano orogeny (Daly et al., 2014), the last major tectonic event of the predepositional history. Nonetheless, a few zircon grains (<10%) record ages younger than 200 Ma and indicate a thermal influence of the upper intrusion (Sardinha Formation), but they also record the influence of the older intrusion in the basin, the Mosquito Formation (ca. 200 Ma). Sample CX46 records a ZFT central

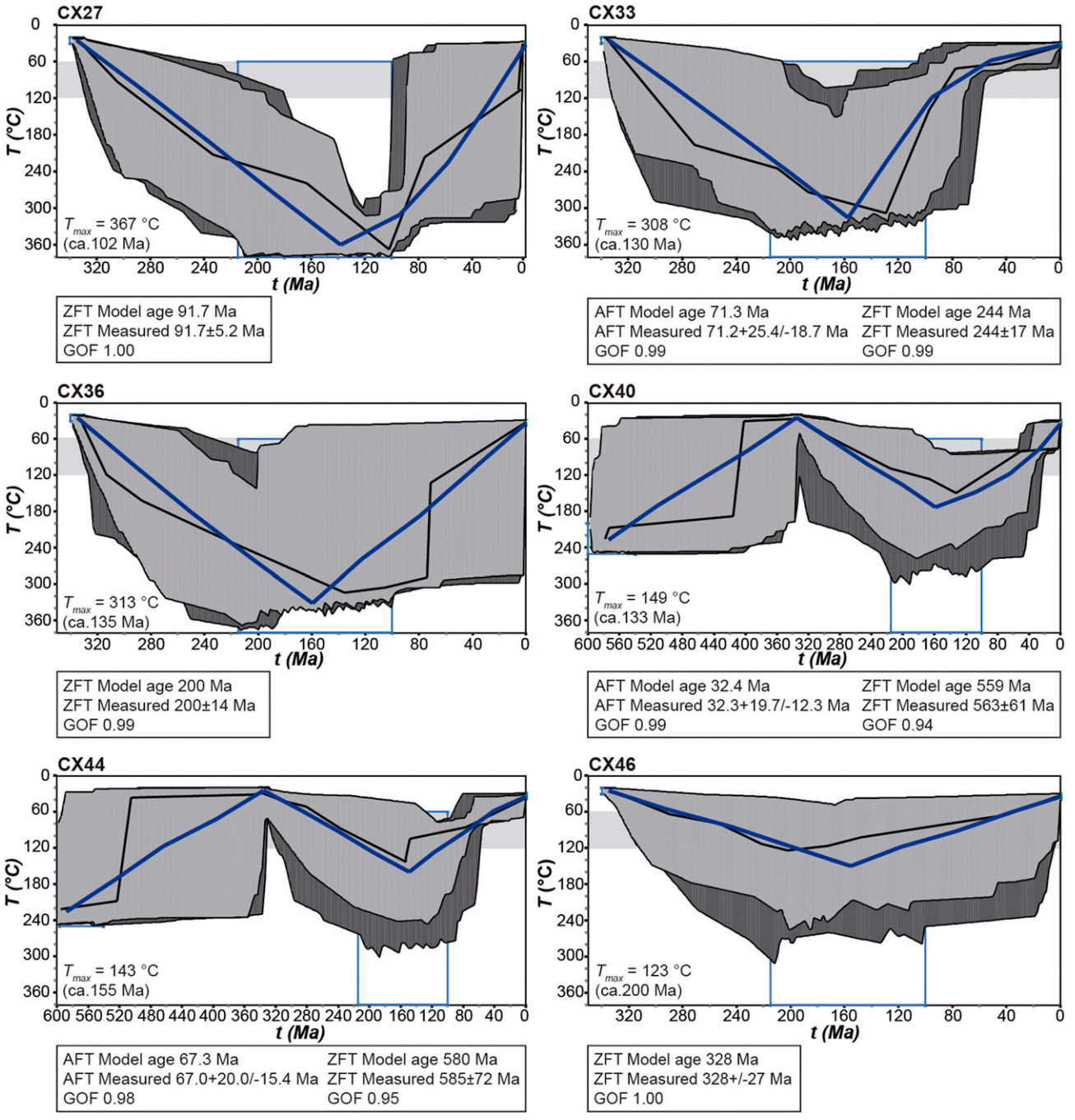

Figure 7. Thermal histories models from HeFTy software (Ketcham, 2005) for borehole caixa (box) samples (CX). Dark-gray, medium-gray, and blue lines represent acceptable, good, and weighted mean fitting time–temperature (*t–T*) paths, respectively. Light-gray boxes indicate the apatite partial annealing zone. Blue boxes are *t–T* constraints. AFT = apatite fission track; GOF = goodness of fit; T_{max} = maximum temperature; ZFT = zircon fission track.

age of 324 ± 27 Ma, which correlates to the initial depositional age of the Poti Formation. Inversion models of the lower group show that maximum postdepositional temperatures range from approximately 149°C to 123°C (Figure 7). The lowermost sample (CX46) records the maximum paleotemperature related to the Mosquito Formation (ca. 200 Ma), which is associated with the CAMP event that largely affected the Parnaíba Basin (Merle et al., 2011).

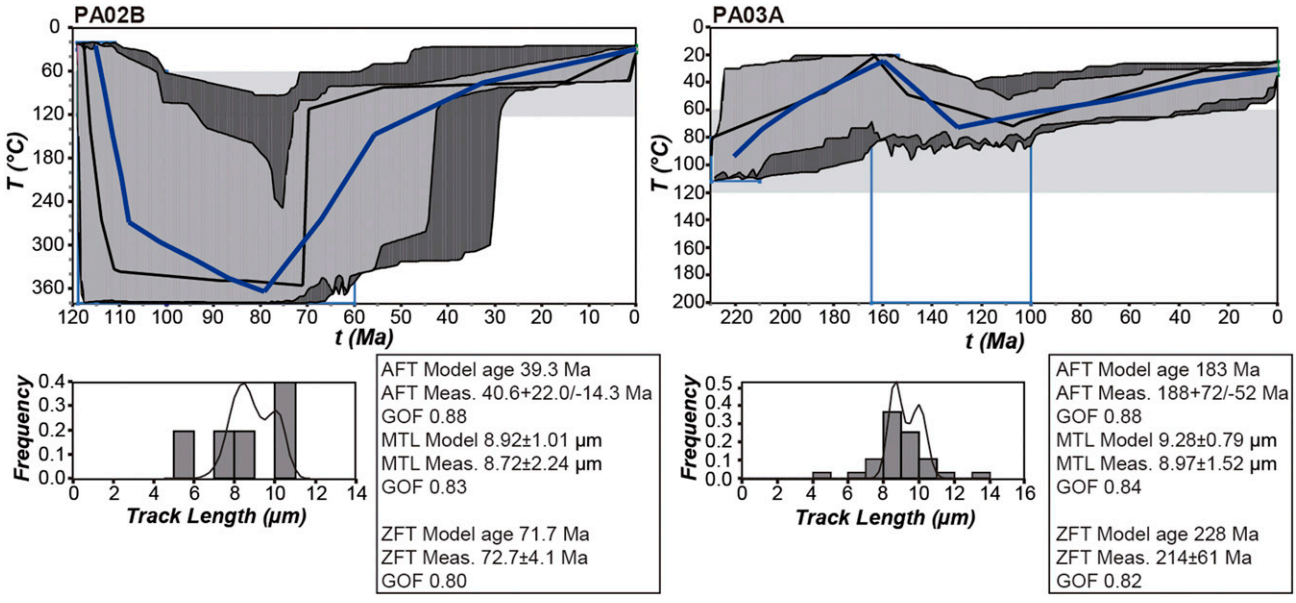

Figure 8. Thermal histories models from HeFTy software (Ketcham, 2005) for Parnaíba Basin outcrop samples (PA). Dark-gray, medium-gray, and blue lines represent acceptable, good, and weighted mean fitting time–temperature (*t–T*) paths, respectively. Light-gray boxes indicate the apatite partial annealing zone. Blue boxes are *t–T* constraints. AFT = apatite fission track; GOF = goodness of fit; Meas. = measured; MTL = mean track length; ZFT = zircon fission track.

Regarding the petroleum system, the maximum paleotemperatures experienced by the upper group samples altered the physical properties of the reservoir rocks in the Parnaíba Basin. Paleotemperatures above 225°C, which were estimated for sandstone potential reservoir layers (upper group, Figure 9) and intruded by later Sardinha Formation magmatism, significantly modified the fabric of these rocks. Reservoir layers that experience these high temperatures underwent hydrocarbon degradation (Vandenbroucke et al., 1999). High temperatures also resulted in hydrothermal fluid percolation and alteration of framework grains (quartz and feldspars). The high-temperature fluids from the intrusion caused almost total feldspar dissolution, increasing the intragranular porosity in the upper group. However, after the thermal influence, fluids rich in carbonate and silica started to precipitate minerals in pore spaces, substantially increasing cementation, as shown in Table 2. Even with porosity enhancement caused by grain dissolution, the formation of carbonate cement is not favorable in a reservoir context because it decreases permeability (Bjørlykke et al., 1989; Poelchau et al., 1997; Ahmed, 2002; Taylor et al., 2010).

In the lower group, a mixture of thermal influence is observed in the maximum paleotemperatures. This is explained by an older high-intensity thermal event related to the Mosquito Formation coming from the lower depths of the basin and a younger influence from the upper intrusion (Sardinha Formation) acting on this group. In terms of paleotemperature, these samples are favorable for hydrocarbon reservoirs because they did not reach temperatures high enough to alter the reservoir layer (>225°C) and result in hydrocarbon degradation. However, diagenetic aspects do not support better petrophysical conditions compared to the upper group. Grain dissolution in the lower group created less secondary porosity probably because of higher mechanical compaction. Porosity of samples shows compact sandstones with less than 10% porosity, an unfavorable condition for reservoir rocks (Table 2), with early illitization and pyrite presence also described in samples from the lower group. According to Rickard (1997), authigenic pyrite forms from 25°C to 125°C. The occurrence of euhedral pyrite in pore space implies low rates of sulfide production during early diagenesis. In contrast, rocks with higher contents of sulfur result in framboidal pyrites after microbial organisms supersaturate the intraporous fluids (Taylor and Macquaker, 2000). In this case, sand-rich rocks of the lower group have low FeS saturation precipitating small, nearly euhedral intrapore pyrite. The absence of pyrite crystals in the upper group

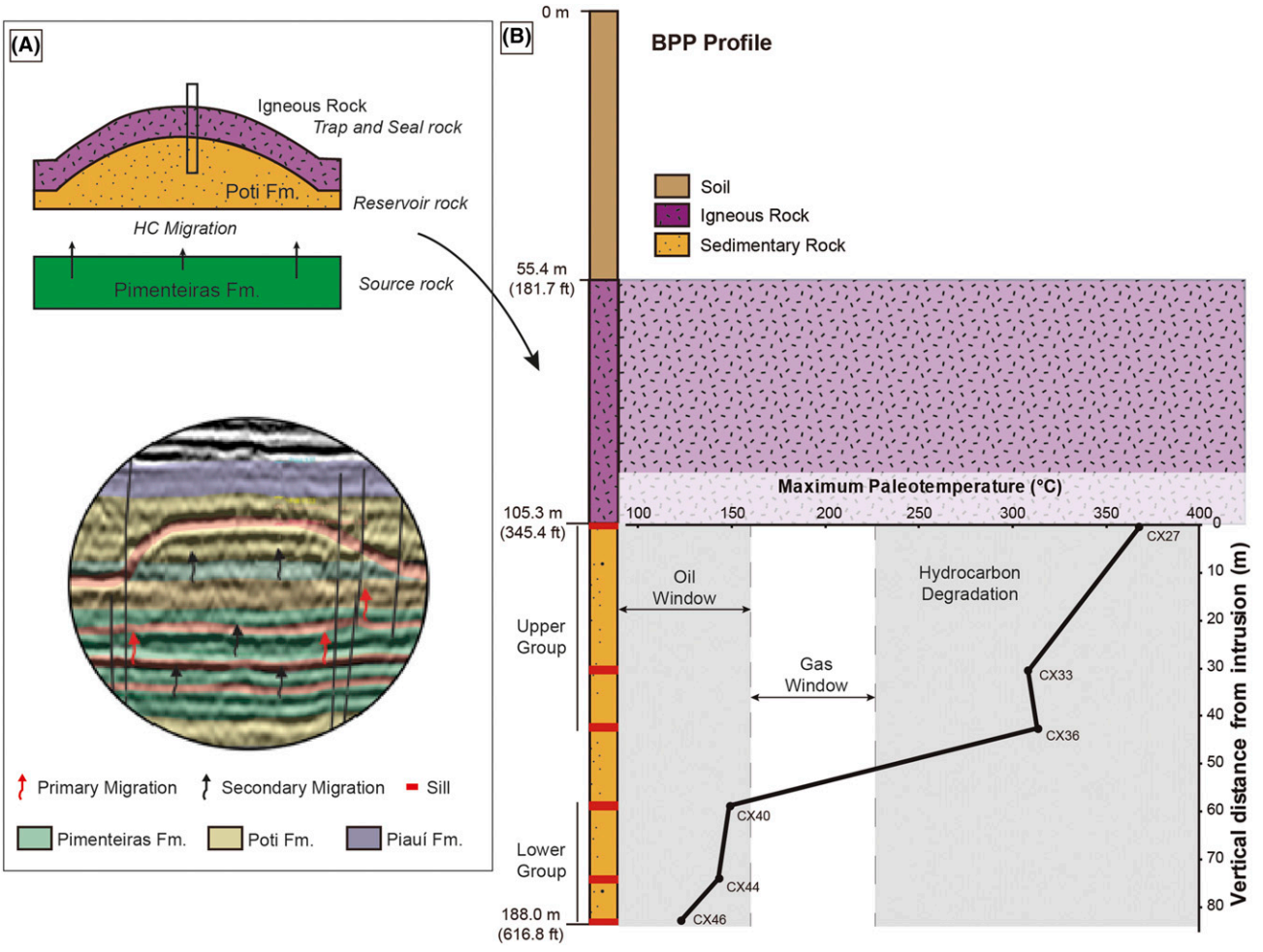

Figure 9. (A) Schematic model of the Pimenteiras–Poti petroleum system with an interpreted seismic representation (modified from de Miranda et al., 2018). (B) Maximum paleotemperature profile for borehole samples. Between samples CX36 and CX40, there is an important decay in the thermal influence from the upper igneous rocks. Below approximately 50 m (~164 ft) from the intrusion, the sedimentary rocks maintained low temperatures and the reservoir layer stayed unmodified. BPP = Bom Princípio/Piauí; CX = borehole caixa (box) sample; Fm. = Formation.

suggests a deficiency in organic matter during early diagenesis or even destabilization of FeS by high paleotemperature fluids in these rocks.

According to the thermochronological data of the reservoir rocks situated under the intrusion, it is possible to separate two heating events in the borehole samples. The deepest and oldest event is recorded in the lower group of sedimentary samples, with some ZFT grain ages circa 200 Ma, correlated to the Mosquito Formation igneous event, but rock samples of this event were not found in the borehole. The younger heating event circa 124 Ma (Sardinha Formation) is recorded in all sedimentary rocks of the borehole and near to the igneous body with maximum paleotemperatures greater than 225°C in the upper group sandstones. To the contrary, the rocks of the lower group did not reach high maximum paleotemperatures (>225°C).

These results impact the unconventional petroleum system of intrusion-triggered maturation described by de Miranda et al. (2018) for the central part of the Parnaíba Basin, which highlights two groups of magmatic sills that intruded the sedimentary rocks. The deepest group was placed in the Pimenteiras Formation (source rocks), which triggered hydrocarbon generation, and the second and shallower group was associated with the Poti and Cabeças Formations (reservoir rocks). The shallower igneous rocks worked as channels for hydrocarbon migration and as stratigraphic traps in places where the saucer-shaped intrusions were positioned over the reservoir rocks.

Thermal History and Petroleum Systems of the Eastern Margin

Along the eastern edge of the Parnaíba Basin, the thermochronological results reveal that all samples were thermally influenced by the two magmatic events, Mosquito (ca. 200 Ma) and Sardinha (120–130 Ma), although the last event is better registered. Two sets of samples were analyzed; those from the BPP borehole record the decay of the thermal influence near an intrusive rock, and the outcrop samples show the regional thermal influence of the magmatic events.

The first set of samples from the Poti Formation supports the thermal influence, allowing for an estimation of thermal decay in the borehole (Figure 9). In contrast, a separate set of samples collected in outcrop far from an intrusive records a predepositional ZFT central age. However, the youngest ZFT age circa 145 Ma represents a zircon grain that has been completely reset by intrusions of the Sardinha Formation and records the regional thermal influence of the last event in this part of the basin.

The Cabeças Formation outcrop sample PA09A records a ZFT central age of provenance; nevertheless, it also records zircon grain ages associated in time with the younger magmatic intrusion (Sardinha Formation) at circa 120 Ma. Petrographic information of this sample shows moderate sorting and more angular and irregular grain shapes, implying shorter grain transport. This sample has higher porosity than the Poti samples (Table 2) and is cemented by opaque ferruginous minerals, indicating a transitional–continental environment with meteoric water percolation and oxidation during diagenesis.

Sample PA03A from the Pastos Bons Formation is interpreted as from a typically low-energy environment with fine quartz and mica grains. The biologic action by trace fossils along with nearly euhedral pyrite minerals are indications of mildly reducing conditions (Worden and Morad, 2003). Euhedral pyrite also indicates low saturation in sulfate (Taylor and Macquaker, 2000). Thermochronological data from this sample show an AFT central age of 130 ± 31 Ma, indicating a major influence from the Sardinha Formation and a maximum paleotemperature of approximately 71°C related to this intrusion (Figure 8).

Stratigraphically above the Pastos Bons Formation, sample PA02B from the Corda Formation shows larger pore spaces than Poti Formation samples. Cementation occurs from carbonate minerals with early illitization of micaceous minerals, and the presence of euhedral, intrapore pyrite resulted from an early diagenetic process. Inversion modeling of the AFT and ZFT data show heating events coeval to deposition (Figure 8). This is not well resolved but represents Corda Formation sandstone deposition associated with an intrusive event of the Sardinha Formation, which explains the correlated deposition and thermal influence of this sample.

In the context of the Parnaíba Basin, the Mosquito and Sardinha Formations strongly affected the sedimentary rocks and surrounding basement rocks. The first event (Mosquito Formation) is associated in time with the large igneous province CAMP (Marzoli et al., 2017; Svensen et al., 2017) that affected the western part of Gondwana during the early stage of paleocontinent breakup. Regionally, in the western basement rocks of the basin (Archean–Paleoproterozoic granites and gneisses), Dias et al. (2017) applied ZFT dating and determined younger ages of circa 200 Ma, reflecting crustal heating associated with the Lower Jurassic Mosquito. Also, Klein et al. (2013) dated intrusions in the São Luís craton in the northwestern edge of the basin, correlated in time to the Mosquito event. These studies show the large extension of CAMP overlying the basement rocks and the Paleozoic basin. In the sedimentary rocks of the Parnaíba Basin, CAMP is linked to the western edge of the basin in which intrusive bodies of the Mosquito Formation are exposed (De Min et al., 2003; Merle et al., 2011; Mocitaiba et al., 2017).

The Sardinha Formation is described in the eastern edge of the basin (Oliveira et al., 2018) and linked to another large igneous province, the Paraná–Etendeka magmatic province, which is associated with the later phase of Gondwana breakup in the southern Atlantic Ocean margin (Mizusaki et al., 2002). This event is connected to diverse intrusive rocks in eastern Brazil, including the Rio Ceará–Mirim Dike Swarm (de Castro et al., 2018) in the eastern basement rocks of the Parnaíba Basin.

Analyzing the reservoir elements in the eastern edge of the Parnaíba Basin, this study verified the thermal influence of the two magmatic events. The samples reveal a greater thermal influence of the Sardinha Formation supported by high PAZ of AFT

(>120°C) and AFT central ages correlated with the last magmatic event. The ZFT central ages record predepositional ages correlated to the Brasiliano orogeny, although ZFT single grain ages evidence the thermal influence of both Mesozoic magmatic events with a higher age proportion associated with the younger Sardinha Formation. The implications of these magmatic events in the Parnaíba Basin are linked with different aspects of the petroleum systems. Magmatic intrusions can act on each of the petroleum system elements in either a positive or negative way. Placement of magmatic rocks close to source rocks can enhance regional and local heat-flow charge in immature basins (Holford et al., 2013; Senger et al., 2017). In the Parnaíba Basin, Rodrigues (1995) and Porto and Pereira (2014) associate the thermal effect on source rock maturation of the Pimenteiras Formation to igneous bodies of the Mosquito Formation. Different authors also discuss the positive effects of intrusion events on migration, traping, and sealing elements in sedimentary basins (Schutter, 2003; Thomaz Filho et al., 2008; Rateau et al., 2013). The placement of saucer-shaped intrusion is shown by de Castro et al. (2018) using seismic data and incorporated by de Miranda et al. (2018) into the petroleum systems of the Parnaíba Basin acting as stratigraphic seal and trap (Figures 9A, 10). The Sardinha event may have also acted on hydrocarbon generation, although the intrusion also altered the reservoir rocks as shown in the borehole samples.

CONCLUSIONS

In this study, the samples allowed the identification of the thermal effects of surrounding igneous rocks on potential gas reservoir rocks. The AFT, ZFT, and petrographic data unravel the intrusions' influence on the reservoir quality, separating zones of enhancement and diminishment of thermal conditions. In this way, intrusions effectively altered the reservoir layers in the eastern part of the Parnaíba Basin. These results validate the fission-track analyses to delimit thermal histories of petroleum systems.

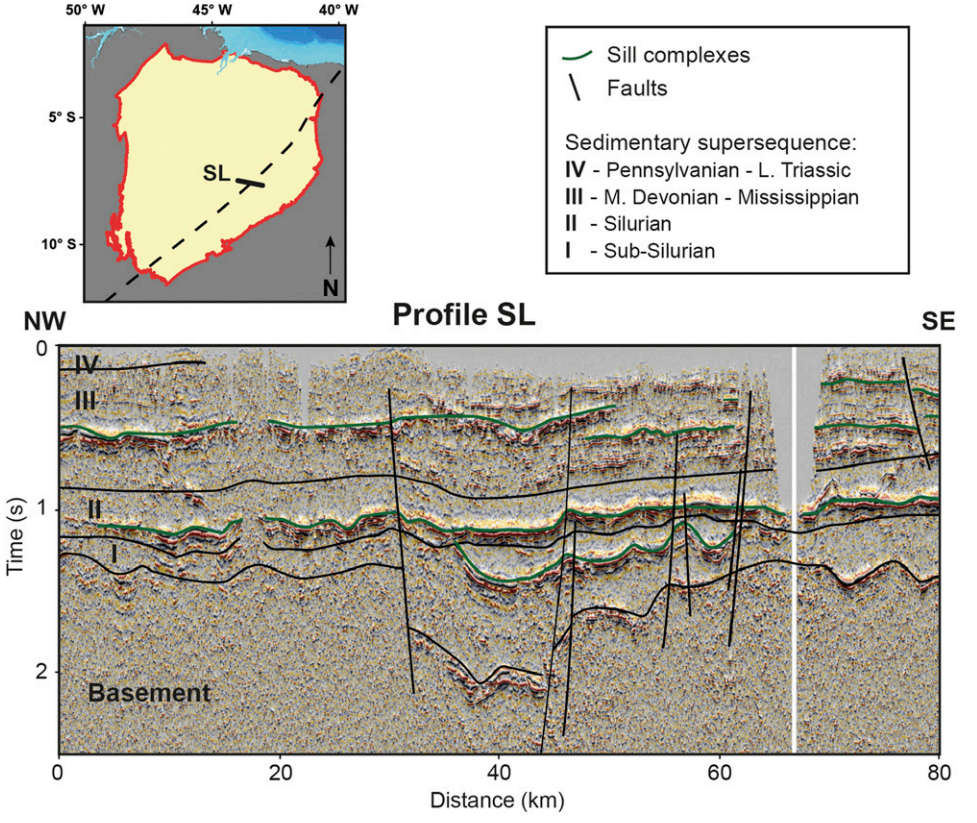

Figure 10. Interpreted seismic line (SL) crosscutting the Transbrasiliano lineament in the eastern edge of the Parnaíba Basin with sill complexes highlighted by green lines (modified from de Castro et al., 2018). L. = Lower; M. = Middle.

The intrusion effects on Poti and Cabeças samples increased grain dissolution, enhancing intragranular porosity because of higher temperature fluid percolation in the system; however, they also increased carbonate precipitation, resulting in low permeability. The Pastos Bons Formation sample was thermally influenced by the intrusion, but the rocks show no diagenetic features or porosity favorable to a potential reservoir. The deposition history of the Corda Formation sample is close in time with the Sardinha intrusion; thus, the duration of the intrusion was short.

Finally, thermochronological data show influences of the Mosquito and Sardinha events, but the major influence in the eastern part of the Parnaíba Basin is related to the Sardinha Formation (ca. 124 Ma). In borehole samples, the material closer than approximately 50 m (~164 ft) to magmatic activity had its reservoir properties obliterated by high temperatures (>225°C), resulting in reservoir and hydrocarbon degradation. In the lower group of borehole samples, the interval farther than approximately 50 m (~164 ft) from the intrusion, the maximum paleotemperatures were sufficiently low that potential reservoir layers remained thermally unaltered.

REFERENCES CITED

Agência Nacional do Petróleo, Gás Natural e Biocombustíveis, 2015, Bacia do parnaíba: Sumário geológico e setores em oferta—13ª Rodada de licitações, accessed October 15, 2017, http://www.anp.gov.br/.

Agência Nacional do Petróleo, Gás Natural e Biocombustíveis, 2017, Boletim da produção de petróleo e gás natural—Circulação externa. Setembro 2017/ Número 85, accessed October 18, 2017, http://www.anp.gov.br/.

Ahmed, W., 2002, Effects of heat-flow and hydrothermal fluids from volcanic intrusions on authigenic mineralization in sandstone formations: Bulletin of the Chemical Society of Ethiopia, v. 16, no. 1, p. 37–52, doi:10.4314/bcse.v16i1.20947.

Allen, P. A., and J. R. Allen, 2013, Basin analysis: Principles and application to petroleum play assessment: Oxford, England, John Wiley & Sons, 632 p.

Almeida, F. F. M., and C. D. R. Carneiro, 2004, Inundações marinhas fanerozóicas no Brasil e recursos minerais associados, *in* V. Mantesso-Neto, A. Bartorelli, C. D. R. Carneiro, and B. B. Brito-Neves, eds., Geologia do continente sul-americano: Evolução da obra de Fernando Flávio Marques de Almeida: São Paulo, Beca, p. 43–58.

Araújo, R. N., A. C. R. Nogueira, J. Bandeira, and R. S. Angélica, 2016, Shallow lacustrine system of the Permian Pedra de Fogo Formation, Western Gondwana, Parnaíba Basin, Brazil: Journal of South American Earth Sciences, v. 67, p. 57–70, doi:10.1016/j.jsames.2016.01.009.

Armstrong, P. A., 2005, Thermochronometers in sedimentary basins: Reviews in Mineralogy and Geochemistry, v. 58, no. 1, p. 499–525, doi:10.2138/rmg.2005.58.19.

Baksi, A. K., and D. A. Archibald, 1997, Mesozoic igneous activity in the Maranhão province, northern Brazil: $^{40}Ar/^{39}Ar$ evidence for separate episodes of basaltic magmatism: Earth and Planetary Science Letters, v. 151, no. 3–4, p. 139–153, doi:10.1016/S0012-821X(97)81844-4.

Becker, R. T., 1993, Anoxia, eustatic changes, and Upper Devonian to lowermost Carboniferous global ammonoid diversity, *in* M. R. House, ed., The Ammonoidea: Environment, ecology, and evolutionary change: Oxford, England, Oxford University Press, p. 115–164.

Bernet, M., and J. I. Garver, 2005, Fission-track analysis of detrital zircon: Reviews in Mineralogy and Geochemistry, v. 58, no. 1, p. 205–237, doi:10.2138/rmg.2005.58.8.

Bjørlykke, K., M. Ramm, and G. C. Saigal, 1989, Sandstone diagenesis and porosity modification during basin evolution: Geologische Rundschau, v. 78, no. 1, p. 243–268, doi:10.1007/BF01988363.

Brown, R., K. Gallagher, and M. Duane, 1994, A quantitative assessment of the effects of magmatism on the thermal history of the Karoo sedimentary sequence: Journal of African Earth Sciences, v. 18, no. 3, p. 227–243, doi:10.1016/0899-5362(94)90007-8.

Burke, K., D. S. MacGregor, and N. R. Cameron, 2003, Africa's petroleum systems: Four tectonic "Aces" in the past 600 million years: Geological Society, London, Special Publications 2003, v. 207, p. 21–60, doi:10.1144/GSL.SP.2003.207.3.

Carter, A., 2007, Chapter 33: Heavy minerals and detrital fission-track thermochronology: Developments in Sedimentology, v. 58, p. 851–868, doi:10.1016/S0070-4571(07)58033-7.

Cunha, P. R., A. R. Bianchini, J. L. Caldeira, and C. C. Martins, 2012, Parnaíba Basin—The awakening of a giant: 11th Simposio Bolivariano Exploración Petrolera en las Cuencas Subandinas, Cartagena, Colombia, July 29–August 1, 2012.

Daly, M. C., V. Andrade, C. A. Barousse, R. Costa, K. McDowell, N. Piggott, and A. J. Poole, 2014, Brasiliano crustal structure and the tectonic setting of the Parnaíba basin of NE Brazil: Results of a deep seismic reflection profile: Tectonics, v. 33, no. 11, p. 2102–2120, doi:10.1002/2014TC003632.

de Brito Neves, B. B., 2002, Main stages of the development of the sedimentary basins of South America and their relationship with the tectonics of supercontinents: Gondwana Research, v. 5, no. 1, p. 175–196, doi:10.1016/S1342-937X(05)70901-1.

de Castro, D. L., F. H. R. Bezerra, R. A. Fuck, and R. M. Vidotti, 2016, Geophysical evidence of pre-sag rifting and post-rifting fault reactivation in the Parnaíba basin, Brazil: Solid Earth, v. 7, no. 2, p. 529–548, doi:10.5194/se-7-529-2016.

de Castro, D. L., R. A. Fuck, J. D. Phillips, R. M. Vidotti, F. H. Bezerra, and E. L. Dantas, 2014, Crustal structure beneath the Paleozoic Parnaíba Basin revealed by airborne gravity and magnetic data, Brazil: Tectonophysics, v. 614, p. 128–145, doi:10.1016/j.tecto.2013.12.009.

de Castro, D. L., D. C. Oliveira, and M. H. B. Hollanda, 2018, Geostatistical interplay between geophysical and geochemical data: Mapping litho-structural assemblages of Mesozoic igneous activities in the Parnaíba Basin (NE Brazil): Surveys in Geophysics, v. 39, no. 4, p. 683–713, doi:10.1007/s10712-018-9463-5.

Della Fávera, J. C., 1990, Tempestitos da Bacia do Parnaíba, Ph.D. thesis, Instituto de Geociências/Universidade Federal do Rio Grande do Sul, Porto Alegre, Brazil, 243 p.

De Min, A., E. M. Piccirillo, A. Marzoli, G. Bellieni, P. R. Renne, M. Ernesto, and L. S. Marques, 2003, The Central Atlantic Magmatic Province (CAMP) in Brazil: Petrology, geochemistry, $^{40}Ar/^{39}Ar$ ages, paleomagnetism and geodynamic implications, *in* W. Hames, J. G. McHone, P. C. Renne, and C. Ruppel, eds., The Central Atlantic Magmatic Province: Insights from fragments of Pangea: American Geophysical Union, Washington, DC, Geophysical Monograph Series 136, p. 91–128, doi:10.1029/136GM06.

de Miranda, F. S., P. R. Cunha, J. Caldeira, F. Aragão, and D. Michelon, 2016, The atypical igneous-sedimentary petroleum systems of the Parnaíba basin: Seismic, well-logs and analogues: International Conference and Exhibition, Barcelona, Spain, April 3–6, 2016, p. 220, doi:10.1190/ice2016-6471370.1.

de Miranda, F. S., A. L. Vettorazzi, P. R. da Cruz Cunha, F. B. Aragão, D. Michelon, J. L. Caldeira, E. Porsche, et al., 2018, Atypical igneous-sedimentary petroleum systems of the Parnaíba Basin, Brazil: Seismic, well logs and cores: Geological Society, London, Special Publications 2018, v. 472, no. 1, p. 341–360, doi:10.1144/SP472.15.

de Oliveira, D. C., and W. U. Mohriak, 2003, Jaibaras trough: An important element in the early tectonic evolution of the Parnaíba interior sag basin, Northern Brazil: Marine and Petroleum Geology, v. 20, no. 3–4, p. 351–383, doi:10.1016/S0264-8172(03)00044-8.

Dias, A. N. C., C. A. V. Moura, J. M. Neto, F. Chemale Jr., T. J. Girelli, and K. M. Masuyama, 2017, Geochronology and thermochronology of the gneisses of the Brasiliano/Pan-African Araguaia Belt: Records of exhumation of West Gondwana and Pangea break up: Journal of South American Earth Sciences, v. 80, p. 174–191, doi:10.1016/j.jsames.2017.09.027.

Dickinson, W. R., L. S. Beard, G. R. Brakenridge, J. L. Erjavec, R. C. Ferguson, K. F. Inman, R. A. Knepp, F. A. Lindberg, and P. T. Ryberg, 1983, Provenance of North America Phanerozoic sandstones in relation to tectonic setting: Geological Society of America Bulletin, v. 94, no. 2, p. 222–235, doi:10.1130/0016-7606(1983)94<222:PONAPS>2.0.CO;2.

Donelick, R. A., P. B. O'Sullivan, and R. A. Ketcham, 2005, Apatite fission-track analysis: Reviews in Mineralogy and Geochemistry, v. 58, no. 1, p. 49–94, doi:10.2138/rmg.2005.58.3.

Dumitru, T. A., 1993, A new computer-automated microscope stage system for fission-track analysis: Nuclear Tracks and Radiation Measurements, v. 21, no. 4, p. 575–580, doi:10.1016/1359-0189(93)90198-I.

Engelmann de Oliveira, C. H., A. R. Jelinek, F. Chemale Jr., and J. A. Cupertino, 2016, Thermotectonic history of the southeastern Brazilian margin: Evidence from apatite fission track data of the offshore Santos Basin and continental basement: Tectonophysics, v. 685, no. 20, p. 21–34, doi:10.1016/j.tecto.2016.07.012.

Fodor, R. V., A. N. Sial, S. B. Mukasa, and E. H. McKee, 1990, Petrology, isotope characteristics, and K-Ar ages of the Maranhao, northern Brazil, Mesozoic basalt province: Contributions to Mineralogy and Petrology, v. 104, no. 5, p. 555–567, doi:10.1007/BF00306664.

Galbraith, R. F., and G. M. Laslett, 1993, Statistical models for mixed fission track ages: Nuclear Tracks and Radiation Measurements, v. 21, no. 4, p. 459–470, doi:10.1016/1359-0189(93)90185-C.

Gleadow, A. J., and C. Seiler, 2015, Fission track dating and thermochronology, *in* W. J. Rink and J. W. Thompson, eds, Encyclopedia of scientific dating methods: Dordrecht, the Netherlands, Springer, p. 285–296, doi:10.1007/978-94-007-6304-3_5.

Góes, A. M. O., 1995, Formação Poti (Carbonífero inferior) da Bacia do Parnaíba, Ph.D. thesis, Universidade de São Paulo, São Paulo, Brazil, 204 p.

Góes, A. M. O., and F. J. Feijó, 1994, Bacia do Parnaíba: Boletim de Geociências da Petrobras, v. 8, no. 1, p. 57–67.

Góes, A. M. O., J. M. P. Souza, and U. B. Teixeira, 1990, Estágio exploratório e perspectivas petrolíferas da bacia do Parnaíba: Boletim de Geociências da Petrobras, v. 4, no. 1, p. 55–64.

Green, P. F., 1981, A new look at statistics in fission-track dating: Nuclear Tracks, v. 5, no. 1–2, p. 77–86, doi:10.1016/0191-278X(81)90029-9.

Green, P. F., P. V. Crowhurst, and I. R. Duddy, 2004, Integration of AFTA and (U-Th)/He thermochronology to enhance the resolution and precision of thermal history reconstruction in the Anglesea-1 well, Otway Basin, SE Australia: Eastern Australasian Basins Symposium (EABS), Adelaide, Australia, September 19–22, 2004, p. 117–131.

Heilbron, M., E. Guedes, M. Mane, C. de Morisson Valeriano, M. Tupinambá, J. Almeida, L. G. do Eirado Silva, B. P. Duarte, J. C. D. Favera, and A. Viana, 2018, Geochemical and temporal provinciality of the magmatism of the eastern Parnaíba Basin, NE Brazil: Geological Society, London, Special Publications 2018, v. 472, p. 251–278, doi:10.1144/SP472.11.

Holford, S. P., N. Schofield, C. L. Jackson, C. Magee, P. F. Green, and I. R. Duddy, 2013, Impacts of igneous intrusions on source reservoir potential in prospective sedimentary basins along the western Australian continental margin: West Australian Basins Symposium, Perth, Australia, August 18–21, 2013, 12 p.

Houseknecht, D. W., 1988, Intergranular pressure solution in four quartzose sandstones: Journal of Sedimentary Research, v. 58, no. 2, p. 228–246, doi:10.1306/212F8D64-2B24-11D7-8648000102C1865D.

Hurford, A. J., 1990, Standardization of fission track dating calibration: Recommendation by the Fission Track Working Group of the IUGS Subcommission on Geochronology: Chemical Geology: Isotope Geoscience Section, v. 80, no. 2, p. 171–178, doi:10.1016/0168-9622(90)90025-8.

Hurford, A. J., and P. F. Green, 1983, The zeta age calibration of fission-track dating: Chemical Geology, v. 41, p. 285–317, doi:10.1016/S0009-2541(83)80026-6.

Ketcham, R. A., 2005, Forward and inverse modeling of low-temperature thermochronometry data: Reviews in Mineralogy and Geochemistry, v. 58, no. 1, p. 275–314, doi:10.2138/rmg.2005.58.11.

Ketcham, R. A., A. Carter, R. A. Donelick, J. Barbarand, and A. J. Hurford, 2007, Improved modeling of fission-track annealing in apatite: American Mineralogist, v. 92, no. 5–6, p. 799–810, doi:10.2138/am.2007.2281.

Kingston, J., and J. R. Matzko, 1995, Undiscovered petroleum of the Brazilian interior sag basins: International Geology Review, v. 37, no. 11, p. 959–980, doi:10.1080/00206819509465435.

Klein, E. L., R. S. Angélica, C. Harris, F. Jourdan, and M. Babinski, 2013, Mafic dykes intrusive into Pre-Cambrian rocks of the São Luís cratonic fragment and Gurupi Belt (Parnaíba Province), north–northeastern Brazil: Geochemistry, Sr–Nd–Pb–O isotopes, $^{40}Ar/^{39}Ar$ geochronology, and relationships to CAMP magmatism: Lithos, v. 172–173, p. 222–242, doi:10.1016/j.lithos.2013.04.015.

Linol, B., M. J. de Wit, C. H. Kasanzu, R. da Silva Schmitt, F. J. Corrêa-Martins, and A. Assis, 2016, Correlation and paleogeographic reconstruction of the Cape-Karoo basin sequences and their equivalents across central west Gondwana, *in* B. Linol and M. de Wit, eds., Origin and evolution of the Cape Mountains and Karoo Basin: Berlin, Springer, Regional Geology Reviews, p. 183–192, doi:10.1007/978-3-319-40859-0_18.

Magoon, L. B., and W. G. Dow, 1994, The petroleum system: From source to trap: AAPG Memoir 60, 655 p.

Marzoli, A., S. Callegaro, J. Dal Corso, J. H. Davies, M. Chiaradia, N. Youbi, H. Bertrand, L. Reisberg, R. Merle, and F. Jourdan, 2017, The Central Atlantic Magmatic Province (CAMP): A review, *in* L. Tanner, ed., The Late Triassic world: Topics in geobiology: Berlin, Springer, v. 46, p. 91–125, doi:10.1007/978-3-319-68009-5_4.

Marzoli, A., P. R. Renne, E. M. Piccirillo, M. Ernesto, G. Bellieni, and A. De Min, 1999, Extensive 200-million-year-old continental flood basalts of the Central Atlantic Magmatic Province: Science, v. 284, no. 5414, p. 616–618, doi:10.1126/science.284.5414.616.

Merle, R., A. Marzoli, H. Bertrand, L. Reisberg, C. Verati, C. Zimmermann, M. Chiaradia, G. Bellieni, and M. Ernesto, 2011, $^{40}Ar/^{39}Ar$ ages and Sr–Nd–Pb–Os geochemistry of CAMP tholeiites from Western Maranhão basin (NE Brazil): Lithos, v. 122, no. 3–4, p. 137–151, doi:10.1016/j.lithos.2010.12.010.

Milani, E. J., and P. V. Zalán, 1999, An outline of the geology and petroleum systems of the Paleozoic interior basins of South America: Episodes, v. 22, p. 199–205.

Mizusaki, A. M. P., A. Thomaz-Filho, E. J. Milani, and P. De Césero, 2002, Mesozoic and Cenozoic igneous activity and its tectonic control in northeastern Brazil: Journal of South American Earth Sciences, v. 15, no. 2, p. 183–198, doi:10.1016/S0895-9811(02)00014-7.

Mocitaiba, L. S. R., D. L. de Castro, and D. C. de Oliveira, 2017, Cartografia geofísica regional do magmatismo mesozoico na Bacia do Parnaíba: Geologia USP: Série Científica, v. 17, no. 2, p. 169–192, doi:10.11606/issn.2316-9095.v17-455.

Nomade, S., K. B. Knight, E. Beutel, P. R. Renne, C. Verati, G. Féraud, A. Marzoli, N. Youbi, and H. Bertrand, 2007, Chronology of the Central Atlantic Magmatic Province: Implications for the Central Atlantic rifting processes and the Triassic–Jurassic biotic crisis: Palaeogeography, Palaeoclimatology, Palaeoecology, v. 244, no. 1–4, p. 326–344, doi:10.1016/j.palaeo.2006.06.034.

Oliveira, A. L., M. M. Pimentel, R. A. Fuck, and D. C. Oliveira, 2018, Petrology of Jurassic and Cretaceous basaltic formations from the Parnaíba Basin, NE Brazil: Correlations and associations with large igneous provinces: Geological Society, London, Special Publications 2018, v. 472, p. 279–308, doi:10.1144/SP472.21.

Poelchau, H. S., D. R. Baker, T. Hantschel, B. Horsfield, and B. Wygrala, 1997, Basin simulation and the design of the conceptual basin model, *in* D. H. Welte, B. Horsfield, and D. R. Baker, eds., Petroleum and basin evolution: Insights from petroleum geochemistry, geology and basin modeling: Berlin, Springer Science & Business Media, p. 3–70, doi:10.1007/978-3-642-60423-2_2.

Porto, A. L., and E. Pereira, 2014, Seismic interpretation of igneous intrusions and their implications for an unconventional petroleum system in southeastern Parnaíba Basin, northeastern Brazil: American Geophysical Union Fall Meeting, San Francisco, December 15–19, 2014, abstract V51B-4753.

Rahn, M. K., M. T. Brandon, G. E. Batt, and J. I. Garver, 2004, A zero-damage model for fission-track annealing in zircon: American Mineralogist, v. 89, no. 4, p. 473–484, doi:10.2138/am-2004-0401.

Rateau, R., N. Schofield, and M. Smith, 2013, The potential role of igneous intrusions on hydrocarbon migration, West of Shetland: Petroleum Geoscience, v. 19, no. 3, p. 259–272, doi:10.1144/petgeo2012-035.

Rickard, D., 1997, Kinetics of pyrite formation by the H_2S oxidation of iron (II) monosulfide in aqueous solutions between 25 and 125°C: The rate equation: Geochimica et Cosmochimica Acta, v. 61, no. 1, p. 115–134, doi:10.1016/S0016-7037(96)00321-3.

Rodrigues, R., 1995, A geoquímica orgânica na Bacia do Parnaíba, Ph.D. thesis, Instituto de Geociências/Universidade Federal do Rio Grande do Sul, Porto Alegre, Brazil, 252 p.

Schutter, S. R., 2003, Hydrocarbon occurrence and exploration in and around igneous rocks: Geological Society, London, Special Publications 2003, v. 214, p. 7–33, doi:10.1144/GSL.SP.2003.214.01.02.

Scotese, C. R., R. K. Bambach, C. Barton, R. Van der Voo, and A. M. Ziegler, 1979, Paleozoic base maps: Journal of Geology, v. 87, no. 3, p. 217–277, doi:10.1086/628416.

Senger, K., J. Millett, S. Planke, K. Ogata, C. H. Eide, M. Festøy, O. Galland, and D. A. Jerram, 2017, Effects of igneous intrusions on the petroleum system: A review: First Break, v. 35, no. 6, p. 47–56, doi:10.3997/1365-2397.2017011.

Silva, A. G. D., C. N. D. Almeida, S. D. C. Valente, and L. F. B. D. Almeida, 2017, The petrogenesis of tholeiitic diabases in eastern Parnaíba Basin: Evidence for geochemical heterogeneities in the subcontinental lithospheric mantle in NE Brazil: Brazilian Journal of Geology, v. 47, no. 1, p. 109–126, doi:10.1590/2317-4889201720160041.

Svensen, H. H., T. H. Torsvik, S. Callegaro, L. Augland, T. H. Heimdal, D. A. Jerram, S. Planke, and E. Pereira, 2017, Gondwana large igneous provinces: Plate reconstructions, volcanic basins and sill volumes: Geological Society, London, Special Publications 2017, v. 463, p. 17–40, doi:10.1144/SP463.7.

Tagami, T., and P. B. O'Sullivan, 2005, Fundamentals of fission track thermochronology: Reviews in Mineralogy and Geochemistry, v. 58, no. 1, p. 19–47, doi:10.2138/rmg.2005.58.2.

Taylor, K. G., and J. H. S. Macquaker, 2000, Early diagenetic pyrite morphology in a mudstone-dominated succession: The Lower Jurassic Cleveland Ironstone Formation, eastern England: Sedimentary Geology, v. 131, no. 1–2, p. 77–86, doi:10.1016/S0037-0738(00)00002-6.

Taylor, T. R., M. R. Giles, L. A. Hathon, T. N. Diggs, N. R. Braunsdorf, G. V. Birbiglia, M. G. Kittridge, C. I. Macaulay, and I. S. Espejo, 2010, Sandstone diagenesis and reservoir quality prediction: Models, myths, and reality: AAPG Bulletin, v. 94, no. 8, p. 1093–1132, doi:10.1306/04211009123.

Thomaz Filho, A., A. M. P. Mizusaki, and L. Antonioli, 2008, Magmatism and petroleum exploration in the Brazilian Paleozoic basins: Marine and Petroleum Geology, v. 25, no. 2, p. 143–151, doi:10.1016/j.marpetgeo.2007.07.006.

Thomaz Filho, A., A. M. P. Mizusaki, E. J. Milani, and P. de Cesero, 2000, Rifting and magmatism associated with the South America and Africa break up: Brazilian Journal of Geology, v. 30, no. 1, p. 17–19.

Vandenbroucke, M., F. Behar, and J. L. Rudkiewicz, 1999, Kinetic modeling of petroleum formation and cracking: Implications from the high pressure/high temperature Elgin Field (UK, North Sea): Organic Geochemistry, v. 30, no. 9, p. 1105–1125, doi:10.1016/S0146-6380(99)00089-3.

Vaz, P. T., N. G. A. M. Rezende, J. R. Wanderley Filho, and W. S. Travassos, 2007, Bacia do Parnaíba: Boletim de Geociências da Petrobras, v. 15, no. 2, p. 253–263.

Verdel, C., B. A. van der Pluijm, and N. Niemi, 2012, Variation of illite/muscovite $^{40}Ar/^{39}Ar$ age spectra during progressive low-grade metamorphism: An example from the US Cordillera: Contributions to Mineralogy and Petrology, v. 164, no. 3, p. 521–536, doi:10.1007/s00410-012-0751-7.

Vermeesch, P., 2009, RadialPlotter: A Java application for fission track, luminescence and other radial plots: Radiation Measurements, v. 44, no. 4, p. 409–410, doi:10.1016/j.radmeas.2009.05.003.

Vieira, L. V., and C. M. S. Scherer, 2017, Facies architecture and high resolution sequence stratigraphy of an aeolian, fluvial and shallow marine system in the Pennsylvanian Piauí Formation, Parnaíba Basin, Brazil: Journal of South American Earth Sciences, v. 76, p. 238–256, doi:10.1016/j.jsames.2017.03.009.

Wagner, G., and P. Van den haute, 1992, Fission-track dating: Berlin, Springer Science & Business Media, 285 p.

Welte, D. H., B. Horsfield, and D. R. Baker, 2012, Petroleum and basin evolution: Insights from petroleum geochemistry, geology and basin modeling: Berlin, Springer Science & Business Media, 535 p.

Wilkinson, M., K. L. Milliken, and R. S. Haszeldine, 2001, Systematic destruction of K-feldspar in deeply buried rift and passive margin sandstones: Journal of the Geological Society, v. 158, no. 4, p. 675–683, doi:10.1144/jgs.158.4.675.

Worden, R. H., and S. Morad, 2003, Clay minerals in sandstones: Controls on formation, distribution and evolution, *in* R. H. Worden and S. Morad, eds., Clay mineral cements in sandstones: Hoboken, New Jersey, Blackwell Publishing, p. 1–41, doi:10.1002/9781444304336.ch1.

Yalçin, M. N., R. Littke, and R. F. Sachsenhofer, 1997, Thermal history of sedimentary basins, *in* D. H. Welte, B. Horsfield, and D. R. Baker, eds., Petroleum and basin evolution: Insights from petroleum geochemistry, geology and basin modeling: Berlin, Springer Science & Business Media, p. 71–167, doi:10.1007/978-3-642-60423-2_3.

Zalán, P. V., 2004, Evolução fanerozóica das bacias sedimentares brasileiras, *in* V. Mantesso-Neto, A. Bartorelli, C. D. R. Carneiro, and B. B. Brito-Neves, eds., Geologia do continente sul-americano: Evolução da obra de Fernando Flávio Marques de Almeida: São Paulo, Brazil, Beca, p. 595–613.